PHYSICAL REVIEW D VOLUME 47, NUMBER 4 15 FEBRUARY 1993

Three-dimensional initial data for the collision of two black holes

Gregory B. Cook
Center for Radiophysics and Space Research and Center for Theory and Simulation in Science and Engineering, Cornell University, Ithaca, New York 14853

Matthew W. Choptuik and Mark R. Dubal
Center for Relativity, University of Texas at Austin, Austin, Texas 78712-1081

Scott Klasky
Center for Relativity, University of Texas at Austin, Austin, Texas 78712-1081 and Center for High Performance Computing, University of Texas Systems, Balcones Research Center, 10100 Burnet Rd., Austin, Texas 78758

Richard A. Matzner and Samuel R. Oliveira*
Center for Relativity, University of Texas at Austin, Austin, Texas 78712-1081
(Received 31 August 1992)

We describe three numerical approaches to the construction of three-dimensional initial data for the collision of two black holes. The first of our approaches involves finite differencing the $3+1$ Hamiltonian constraint equation on a Čadež coordinate grid. The difference equations are then solved via the multigrid algorithm. The second approach also uses finite-difference techniques, but this time on a regular Cartesian coordinate grid. A Cartesian grid has the advantage of having no coordinate singularities. However, constant coordinate lines are not coincident with the throats of the black holes and, therefore, special treatment of the difference equations at these boundaries is required. The resulting equations are solved using a variant of line-successive overrelaxation. The third and final approach we use is a global, spectral-like method known as the multiquadric approximation scheme. In this case functions are approximated by a finite sum of weighted quadric basis functions which are continuously differentiable. We discuss particular advantages and disadvantages of each method and compare their performances on a set of test problems.

PACS number(s): 04.20.Jb, 02.60.Cb, 02.70.Bf, 97.60.Lf

I. INTRODUCTION

A first step in the numerical simulation of binary black-hole systems is the construction of suitable initial data. Generically, this problem is three-dimensional (3D) since the two black holes may have arbitrary positions, radii, spins, and linear momenta. To date, the numerical study of the collision of black holes has been limited to evolutions which start from time-symmetric initial data where the holes start out at rest from a finite separation [1]. Initial data representing two black holes with linear momenta and spin have been constructed [2, 3] for axisymmetric configurations. In this paper, we will explore several techniques for constructing initial-data sets which represent two black holes with arbitrary positions, radii, linear momenta, and spins.

A framework has been erected which is designed to allow for the construction of initial-data sets containing multiple black holes, each with individually specifiable linear and angular momenta [4–6]. This *conformal-imaging approach* is based on the Arnowitt-Deser-Misner (ADM) [7], or $3+1$, decomposition of Einstein's equations, York's conformal and transverse-traceless decomposition of the constraint equations, and a method of imaging applicable to tensors. Application of this approach to the construction of axisymmetric initial-data sets has been extensively explored [3, 8] and we refer the reader to these papers for a detailed discussion. In short, construction of initial data following the conformal-imaging approach consists of two distinct parts. First, the momentum (or vector) constraints are solved analytically in a procedure which fixes the momenta on each hole. A formal, infinite-series solution of the momentum constraints has been worked out by Kulkarni *et al.* [6] and an efficient algorithm for evaluating this solution numerically has been constructed by Cook [3] for the case of two black holes. Second, the Hamiltonian constraint equation (which incorporates the solution of the momentum constraint) must be solved numerically. Such numerical solutions for axisymmetric configurations of two black holes have been explored by Cook [3] and, using a method similar to the conformal-imaging approach, by Thornburg [2].

In this paper, we will explore the construction of 3D initial-data sets for the collision of two black holes using

*Present address: Departmento de Fisica, Universidade de Brasilia, Brazil.

the conformal-imaging approach. As mentioned above, the solution of the momentum constraints for general, 3D configurations of two black holes has already been addressed. Solutions for the momentum constraints were computed using two independently constructed codes (following the semianalytic algorithm outlined in [3]). The two codes produced pointwise agreement to better than parts in 10^{11}, far better than the accuracy required for the source of the Hamiltonian constraint. In addition we numerically differenced the semianalytic momentum solution and verified that it does solve the momentum constraints. This constitutes a validation of the coding for this part of the problem. What remains now is to find effective numerical methods of solving the Hamiltonian constraint. We will describe three different approaches to solving this particular problem. Of the three approaches, two employ finite-difference techniques, one on a regular Cartesian coordinate grid and the other on a Čadež coordinate grid (cf. Cook [3]). The third method is a type of global spectral technique known as the multiquadric (MQ) approximation scheme [9]. This method is essentially "gridless"; however, here it is used to solve the Hamiltonian constraint equation written in Cartesian coordinates.

It is important to emphasize that the codes described in this paper are the product of two different research groups acting independently, and compared on a specified, controlled set of test problems. The results presented here represent an unusual effort of validation of numerical relativity coding, which has been carried out only infrequently in the past [10]. Such rigorous comparisons on specific testbed calculations are essential for accurate, reliable development of relativity codes [11].

We begin in Sec. II with a brief review of the basic quantities and equations associated with the conformal-imaging approach. In Sec. III we describe in detail the three different approaches taken in finding numerical solutions of the Hamiltonian constraint. We first describe the Čadež coordinate approach in Sec. III A, including a description of the full approximation storage (FAS)/block-multigrid algorithm used to solve the finite-difference equations. The second approach, called the Cartesian coordinate approach, is described in Sec. III B. The third and final approach discussed in this paper is called the multiquadric approach and is described in Sec. III C. In Sec. IV, we compare the accuracy and efficiency of the three approaches on a set of test problems. Conclusions and discussion are presented in Sec. V.

II. THE CONFORMAL-IMAGING APPROACH

The conformal-imaging approach provides a well-proven foundation for specifying initial-data sets containing black holes. For a detailed description of this approach, see Ref. [3] and references therein. In short, the vacuum Hamiltonian and momentum constraints are expressed, respectively, as

$$8\bar{\nabla}^2\psi - \psi\bar{R} - \frac{2}{3}\psi^5 K^2 + \psi^{-7}\bar{A}_{ij}\bar{A}^{ij} = 0 \tag{1}$$

and

$$\bar{D}_j\bar{A}^{ij} - \frac{2}{3}\psi^6\bar{\gamma}^{ij}\bar{D}_j K = 0. \tag{2}$$

The physical metric γ_{ij} of the spacelike initial-data hypersurface has been conformally decomposed as $\gamma_{ij} = \psi^4\bar{\gamma}_{ij}$, where ψ is a strictly positive conformal factor and $\bar{\gamma}_{ij}$ is the conformal *background* metric. The extrinsic curvature K_{ij}, describing the embedding of the initial-data hypersurface in the full space-time, has also been decomposed as $K_{ij} = \psi^{-2}\bar{A}_{ij} + \frac{1}{3}\gamma_{ij}K$, where K is the trace of the extrinsic curvature and $\bar{A}_{ij}$ is the trace-free conformal *background* extrinsic curvature. Finally, $\bar{R}$ is the Ricci scalar, $\bar{D}_i$ is the covariant derivative, and $\bar{\nabla}^2$ is the scalar Laplacian, all compatible with the conformal background metric. Note that all quantities with an overbar exist in the conformal background space and are related to similar quantities (without overbars) which exist in the physical space.

To simplify the task of solving these equations, the following choices are made. First, the initial-data hypersurface is taken to be maximally embedded in the space-time so that $K = 0$. Second, the initial-data hypersurface is taken to be conformally flat so that $\bar{\gamma}_{ij} = f_{ij}$, a flat metric. This choice fixes the dynamical degrees of freedom in the metric on the initial hypersurface and simplifies both the Hamiltonian and momentum constraints. With these assumptions, the initial-value equations reduce to the simple form

$$\bar{\nabla}^2\psi = -\frac{1}{8}\psi^{-7}\bar{A}_{ij}\bar{A}^{ij} \tag{3}$$

and

$$\bar{D}_j\bar{A}^{ij} = 0. \tag{4}$$

Note that $\bar{D}_i$ and $\bar{\nabla}^2$ are now the familiar flat-space covariant derivative and scalar Laplacian, respectively.

The topology of the initial-data hypersurface is fixed to be two asymptotically flat, "identical" sheets or universes connected by a throat or Einstein-Rosen bridge [12] for each black hole. The identification of the two sheets is accomplished by imposing an isometry condition on the manifold which must be obeyed by all physical fields. The solution of the momentum constraint (4) under these conditions was found by Kulkarni *et al.* [6] in the form of a formal infinite-series solution generated by a method of images applicable to tensors. For the case of two black holes, an accurate and efficient numerical scheme for evaluating the formal infinite series solution has been found [3]. In constructing a solution of the momentum constraints, values for the radius a_α and coordinate center $\mathbf{C}_\alpha$ of the αth hole are fixed along with its linear momentum $\mathbf{P}_\alpha$ and spin $\mathbf{S}_\alpha$.

Given a solution of the momentum constraints (4), the Hamiltonian constraint (3) can be solved as a quasilinear elliptic boundary-value problem given appropriate boundary conditions. The throats of the black holes $B_\alpha \equiv \{\mathbf{x} : |\mathbf{x} - \mathbf{C}_\alpha| = a_\alpha\}$ are fixed-point sets of the isometry condition and are natural boundaries on which to impose boundary conditions. The isometry condition applied to the physical metric at B_α yields the following boundary condition for the conformal factor:

$$n^i_\alpha \bar{D}_i \psi \Big|_{B_\alpha} = -\frac{\psi}{2r_\alpha}\Big|_{B_\alpha}, \tag{5}$$

where $r_\alpha = |\mathbf{x} - \mathbf{C}_\alpha|$ and $\mathbf{n}_\alpha = (\mathbf{x} - \mathbf{C}_\alpha)/r_\alpha$ (in terms of Cartesian components). The boundary condition at infinity follows directly from asymptotic and conformal flatness:

$$\psi \to 1 \quad \text{as } r \to \infty. \tag{6}$$

In practice, infinity is often not a part of the domain of solution for the conformal factor when numerical solutions are found. Typically, a multipole expansion for the conformal factor truncated at monopole order is used to give an approximate boundary condition [13]

$$\frac{\partial \psi}{\partial r} = \frac{1-\psi}{r}, \tag{7}$$

although higher-order approximate boundary conditions can be derived [3].

III. NUMERICAL SOLUTION OF THE HAMILTONIAN CONSTRAINT

A. The Čadež coordinate approach

The first approach for solving the Hamiltonian constraint for two black holes uses finite-difference methods based on a Čadež coordinate grid. The vast majority of numerical research on the collision of two black holes performed to date has used the Čadež coordinate system [1, 3]. Because this coordinate system has constant coordinate surfaces which are boundary conforming, the set of finite-difference equations which we obtain from the Hamiltonian constraint and its boundary conditions are particularly simple and well behaved. Coupled with a multigrid algorithm for solving the finite-difference equations, this approach yields a solution scheme which is extremely fast, computationally efficient, and very accurate. Because this approach is based on a coordinate system which is highly adapted to the problem at hand, it lacks the flexibility to address problems with more than two black holes. This is not a significant concern. The primary concern with any finite-difference scheme based on Čadež coordinates is that it must deal effectively with coordinate singularities. This is easily done when elliptic problems are being addressed, but has proven to be more challenging when stable evolution schemes for hyperbolic equations are required.

The Čadež coordinate system is a numerically generated coordinate system based on a complex-plane transformation from cylindrical coordinates (see Cook [3] for a detailed description of constructing these coordinates). The three Čadež coordinates (η, ξ, ϕ) are based in cylindrical coordinates. $\eta(\rho, z)$ is a radial-like coordinate and $\xi(\rho, z)$ is an angular coordinate. The azimuthal coordinate ϕ is unchanged from cylindrical coordinates. The coordinate system is logically composed of three regions (see Fig. 1):

$$\text{region 1} \equiv \begin{cases} \eta^+ \le \eta < \eta_s, \\ 0 \le \xi \le \xi_s, \\ 0 \le \phi < 2\pi, \end{cases} \tag{8a}$$

$$\text{region 2} \equiv \begin{cases} \eta^- \le \eta < \eta_s, \\ \xi_s \le \xi \le \pi, \\ 0 \le \phi < 2\pi, \end{cases} \tag{8b}$$

$$\text{region 3} \equiv \begin{cases} \eta_s \le \eta < \infty, \\ 0 \le \xi \le \pi, \\ 0 \le \phi < 2\pi. \end{cases} \tag{8c}$$

This three-region nature is the consequence of a coordinate singularity at (η_s, ξ_s) which itself is a consequence of demanding that constant-η surfaces be coincident with each of the two throats while at the same time demanding that constant-η surfaces surround both holes at large radius. Region 1 surrounds the first hole from the throat at $\eta = \eta^+$ out to the singular point. Region 2 surrounds the second hole from its throat at $\eta = \eta^-$ out to the singular point, and region 3 surrounds both holes outside of the singular point.

Numerical computations will be performed in terms of dimensionless quantities. The radius of the first hole, a_1, is taken to set the fundamental length scale so that, in computational coordinates, the first hole has unit ra-

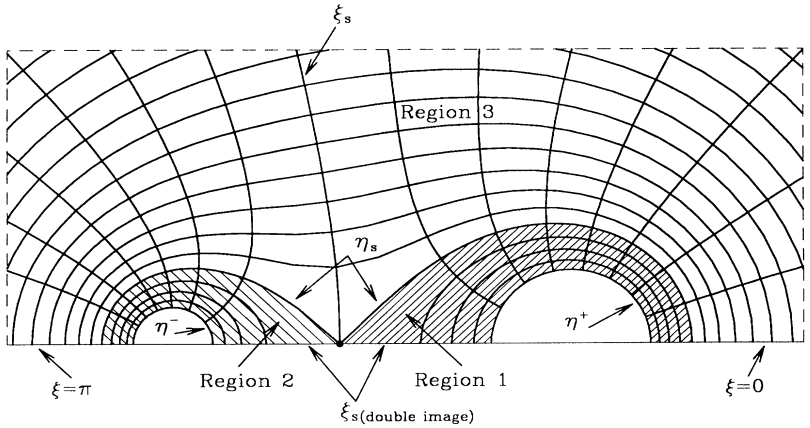

FIG. 1. Čadež coordinates near the two holes showing the *three*-region nature of the coordinate system. (η_s, ξ_s) is the singular point in the coordinate system. $\eta^\pm$ are the constant-coordinate surfaces coincident with the minimal surfaces.

dius. The size of the second hole is parametrized by the dimensionless ratio of the radii of the two holes:

$$\alpha \equiv \frac{a_1}{a_2}. \tag{9}$$

The spatial separation of the two holes is parametrized by

$$\beta \equiv \frac{|\mathbf{C}_1 - \mathbf{C}_2|}{a_1}. \tag{10}$$

These two parameters uniquely define the *background* space configuration of the two holes.

The flat background metric takes the form

$$ds^2 = \frac{a_1^2}{\eta_{,\rho}^2 + \eta_{,z}^2}(d\eta^2 + d\xi^2) + a_1^2\rho^2 d\phi^2, \tag{11}$$

where ρ and z are dimensionless cylindrical coordinates scaled relative to a_1. The Laplacian can be written as

$$\bar{\nabla}^2\psi = \frac{\eta_{,\rho}^2 + \eta_{,z}^2}{a_1^2\rho}\left\{\frac{\partial}{\partial\eta}\left(\rho\frac{\partial\psi}{\partial\eta}\right) + \frac{\partial}{\partial\xi}\left(\rho\frac{\partial\psi}{\partial\xi}\right)\right\} + \frac{1}{a_1^2\rho^2}\frac{\partial^2\psi}{\partial\phi^2}, \tag{12}$$

which is an appropriate form for conservative differencing. The boundary conditions on the two throats (5) take the forms

$$\left[\sqrt{\eta_{,\rho}^2 + \eta_{,z}^2}\frac{\partial\psi}{\partial\eta} + \frac{\psi}{2}\right]_{\eta=\eta^+} = 0 \tag{13}$$

and

$$\left[\sqrt{\eta_{,\rho}^2 + \eta_{,z}^2}\frac{\partial\psi}{\partial\eta} + \frac{\alpha\psi}{2}\right]_{\eta=\eta^-} = 0. \tag{14}$$

Finally, asymptotic flatness is imposed at a boundary at finite radius ($\eta = \eta_f$) via the approximate boundary condition (7), which takes the form

$$\frac{\partial}{\partial\eta}\left[r(\psi - 1)\right]\Big|_{\eta_f} = 0. \tag{15}$$

The presence of the Čadež coordinate singularity and considerations associated with implementing a multigrid solver in conjunction with the three-regioned Čadež coordinate domain suggest that a zone-centered differencing scheme should be used to finite-difference the Hamiltonian constraint. The computational domain will be discretized so that grid points are centered in the following way. The "radial" coordinate η is discretized as

$$\begin{aligned} \eta_i &= (i - \tfrac{1}{2})h_\eta + \eta_s, \\ i &= \begin{cases} -(\mathcal{I}^+ - 1), \ldots, 0 & : \text{region 1}, \\ -(\mathcal{I}^- - 1), \ldots, 0 & : \text{region 2}, \\ 1, \ldots, \mathcal{I} & : \text{region 3}, \end{cases} \\ h_\eta &= \frac{\eta_f - \eta_s}{\mathcal{I}} = \frac{\eta_s - \eta^-}{\mathcal{I}^-} = \frac{\eta_s - \eta^+}{\mathcal{I}^+}. \end{aligned} \tag{16}$$

The same discretization length h_η is possible in both regions 1 and 2 even when the holes are of unequal size because there is freedom in the definition of the Čadež coordinates to place the singular point anywhere along the axis between the holes. The ξ coordinate is not discretized directly but is chosen to be a quadratic function of a new coordinate s in a way which guarantees that grid points are zone centered with the Čadež singularity positioned on an angular zone face even when the holes are of unequal size. The discretization of the ξ coordinate is, thus, given by

$$\begin{aligned} \xi_j &= \xi(s_j) = fs_j^2 + gs_j, \\ s_j &= (j - \tfrac{1}{2})h_s, \qquad j = 1, \ldots, \mathcal{S}^+, \ldots, \mathcal{S}^+ + \mathcal{S}^-, \\ h_s &= \frac{1}{\mathcal{S}^+ + \mathcal{S}^-}, \\ f &= \frac{(\mathcal{S}^+ + \mathcal{S}^-)\pi}{\mathcal{S}^-} - \frac{(\mathcal{S}^+ + \mathcal{S}^-)^2\xi_s}{\mathcal{S}^+\mathcal{S}^-}, \\ g &= \frac{(\mathcal{S}^+ + \mathcal{S}^-)^2\xi_s}{\mathcal{S}^+\mathcal{S}^-} - \frac{\mathcal{S}^+\pi}{\mathcal{S}^-}. \end{aligned} \tag{17}$$

The integers $\mathcal{S}^+$ and $\mathcal{S}^-$ give the number of discrete points above and below ξ_s and must be chosen so that ξ is a monotonically increasing function of s for $0 \le \xi \le \pi$. Finally, the ϕ direction is trivially discretized as

$$\begin{aligned} \phi_k &= (k - \tfrac{1}{2})h_\phi, \\ h_\phi &= \frac{2\pi}{\mathcal{P}}, \\ k &= 1, \ldots, \mathcal{P}, \end{aligned} \tag{18}$$

with the understanding that $\phi_{k+\mathcal{P}} = \phi_k$.

In terms of this discretization, a second-order, conservative finite-difference form of the Hamiltonian constraint (3) can be written as

$$\begin{aligned} &\mathcal{J}_j\left[\rho_{i+\frac{1}{2},j}(\psi_{i+1,j,k} - \psi_{i,j,k}) - \rho_{i-\frac{1}{2},j}(\psi_{i,j,k} - \psi_{i-1,j,k})\right]\frac{h_s h_\phi}{h_\eta} \\ &+ \left[\frac{\rho_{i,j+\frac{1}{2}}}{\mathcal{J}_{j+\frac{1}{2}}}(\psi_{i,j+1,k} - \psi_{i,j,k}) - \frac{\rho_{i,j-\frac{1}{2}}}{\mathcal{J}_{j-\frac{1}{2}}}(\psi_{i,j,k} - \psi_{i,j-1,k})\right]\frac{h_\eta h_\phi}{h_s} \\ &+ \frac{\mathcal{J}_j}{[\rho(\eta_{,\rho}^2 + \eta_{,z}^2)]_{i,j}}(\psi_{i,j,k+1} - 2\psi_{i,j,k} + \psi_{i,j,k-1})\frac{h_\eta h_s}{h_\phi} \\ &+ \frac{\mathcal{J}_j}{8}\psi_{i,j,k}^{-7}(a_1^2\bar{A}_{\ell m}\bar{A}^{\ell m})_{i,j,k}\left(\frac{\rho}{\eta_{,\rho}^2 + \eta_{,z}^2}\right)_{i,j} h_\eta h_s h_\phi = 0, \end{aligned} \tag{19}$$

where $\mathcal{J}_j \equiv \partial\xi/\partial s|_{\xi_j}$ and the background extrinsic curvature $\bar{A}_{\ell m}$ is computed by the techniques discussed in Refs. [3, 14]. Second-order, centered-difference versions of the boundary conditions on the throats are given by

$$\frac{\psi_{i,j,k} - \psi_{i-1,j,k}}{h_\eta} = -\psi_{i,j,k}\left(\frac{2}{4\sqrt{\eta_{,\rho}^2 + \eta_{,z}^2}|_{i-\frac{1}{2},j} - h_\eta}\right) \quad \text{for} \quad i = -(\mathcal{I}^+ - 1), \quad (20)$$

for the throat at $\eta = \eta^+$, and

$$\frac{\psi_{i,j,k} - \psi_{i-1,j,k}}{h_\eta} = -\psi_{i,j,k}\left(\frac{2\alpha}{4\sqrt{\eta_{,\rho}^2 + \eta_{,z}^2}|_{i-\frac{1}{2},j} - \alpha h_\eta}\right) \quad \text{for} \quad i = -(\mathcal{I}^- - 1), \quad (21)$$

for the throat at $\eta = \eta^-$. Finally, a second-order, centered-difference version of the outer boundary condition is given by

$$\frac{\psi_{i+1,j,k} - \psi_{i,j,k}}{h_\eta} = \frac{1 - \psi_{i,j,k}}{h_\eta}\left(1 - \frac{r_{i,j}}{r_{i+1,j}}\right) \quad \text{for} \quad i = \mathcal{I}, \quad (22)$$

where $r_{i,j} \equiv \sqrt{\rho^2 + z^2}|_{i,j}$.

The set of difference equations outlined above yields a large set of coupled, nonlinear algebraic equations which must be solved for the conformal factor ψ. Linearizing this set of equations yields a symmetric, positive-definite, banded system of equations. This linearized system could be solved in a variety of ways, with Newton iterations used to obtain the full, nonlinear solution. Perhaps the most efficient approach for solving such a set of equations, however, is to make use of a FAS-multigrid scheme [15]. Such a scheme can solve a nonlinear boundary-value problem in $O(N)$ operations (where N is the number of equations being solved) and can solve a nonlinear set of equations to a level of accuracy exceeding truncation error, while requiring only the same amount of work needed to solve the linearized system *once* to the same accuracy.

Unfortunately, a standard FAS-multigrid algorithm cannot efficiently accommodate the grid topology of Čadež coordinates. The radial range associated with regions 1 or 2 and region 3 is vastly different. Typically, $(\eta_f - \eta_s)/(\eta_s - \eta^\pm) \sim 10-100$. Multigrid methods achieve their speed and efficiency by solving a given problem using successively coarser grids. Usually, the discretization length (e.g., h_η) for each spatial dimension is doubled in moving to a coarser grid. Eventually, the computational grid is coarsened to the point where there are only a small number of grid points and the equations can be solved very efficiently at this level of discretization. In the case of Čadež coordinates, the radial discretization h_η will quickly reach a point where it cannot be doubled without exceeding $\eta_s - \eta^\pm$. At this point, there may still be a large number of zones in region 3 and a direct solution of the equation at this level would be quite costly.

A solution to this problem is achieved in the following way. Define G_L to be a grid at level L in the multigrid hierarchy, where L is an integer. Let G_f denote the grid with the finest resolution and let G_s denote the coarsest grid on which $h_\eta \le \eta_s - \eta^+$ *and* $h_\eta \le \eta_s - \eta^-$, with $f \ge s \ge 1$. On G_s, the three Čadež regions are "split" and solved in a block-iterative fashion. Regions 1 and 2 on G_s will always contain a relatively small number of grid points and can be solved directly using a standard banded, positive-definite, symmetric matrix solver. Region 3, however, will usually contain too many points to be solved directly and so the FAS-multigrid algorithm is applied to this region independently. The pseudocode below describes the general algorithm used for solving the Čadež-coordinate finite-difference equations and will be referred to as a FAS/block-multigrid procedure.

```
mg_iter = 0
do until (||R_f||_2 < ε||τ_{f-1}||_2 and mg_iter ≥ 2)
  mg_iter = mg_iter + 1
  do L = f ··· s + 1
    Perform 2 smoothing sweeps in regions 1, 2, and
        3 of G_L.
    Compute τ_{L-1} in regions 1, 2, and 3.
    Transfer solution in regions 1, 2, and 3 to G_{L-1}.
  end do
  block_iter = 0
  do until (||R_s||_2 < δ||τ_s||_2 and block_iter ≥ 3)
    block_iter = block_iter + 1
    Find block solution for regions 1 and 2 of G_s via
        direct solution.
    do L = s ··· 2
      Perform 2 smoothing sweeps in region 3 of G_L.
      Compute τ_{L-1} in region 3.
      Transfer solution in region 3 to G_{L-1}.
    end do
    Find block solution for region 3 of G_1 via direct
        solution.
    do L = 2 ··· s
      Compute coarse grid correction in region 3.
      Update solution in region 3 of G_L.
      Perform 2 smoothing sweeps in region 3 of G_L.
    end do
  end do
  do L = s + 1 ··· f
    Compute coarse grid correction in regions 1,
        2, and 3.
    Update solution in regions 1, 2, and 3 of G_L.
    Perform 2 smoothing sweeps in regions 1, 2, and 3
        of G_L.
  end do
end do
```

τ_{L-1} is the relative local truncation error computed between grids G_L and G_{L-1} (cf. Ref. [15]). R_L is the solution residual on G_L which vanishes when the finite-difference equations are solved exactly. $\|R_L\|_2$ and $\|\tau_L\|_2$ are, respectively, the ℓ_2 norms of the residual and relative local truncation error on G_L. And finally, ϵ and δ are appropriate small numbers $0 < \epsilon, \delta < 1$ chosen to achieve satisfactory convergence. Note that for $s < L \le 1$, an inner boundary condition must be supplied for region 3 of G_L since regions 1 and 2 are not approximated on

these grids. This condition is effectively taken to be that $\partial\psi/\partial\eta$ is given by the value on the boundary between region 3 and regions 1 and 2 on G_s. Also, on G_1, region 3 is solved directly using a standard banded, positive-definite, symmetric matrix solver.

B. The Cartesian coordinate approach

The second of our three approaches to the numerical solution of the Hamiltonian constraint for a pair of black holes employs a finite-difference method based on the usual Cartesian coordinates (x, y, z). The algebraic equations which result from finite-differencing in these coordinates are solved by a variant of line-SOR (successive overrelaxation) [16]. Within the context of numerical relativity, we can provide additional motivation for the work described in this subsection. We view the current task of determining black-hole initial data not only as an interesting problem in its own right, but also as a test-bed for approaches and techniques which may prove useful in the *evolution* of the initial data. From this viewpoint, the use of Cartesian coordinates for numerical black-hole work is of substantial interest. First, in contrast to most curvilinear systems which have been used in black-hole studies, these coordinates are manifestly singularity-free, and thus our calculations are free of the coordinate singularities which, historically, have plagued the development of stable algorithms for integrating differenced forms of Einstein's equations. Second, Cartesian coordinates incorporate *no* problem-specific information, as do, for example, Čadež coordinates. At first glance this might seem to be a distinct disadvantage. However, it is likely that a successful treatment of the evolution problem for interacting black holes will be based on incomplete knowledge concerning the location of "inner boundaries" such as the surfaces of isometry used in our formulation of the initial-value problem. Thus, it is of some interest to investigate and develop techniques in numerical relativity for the general treatment of boundaries which are *not* coincident with constant-coordinate surfaces. Finally, Cartesian coordinates tend to minimize the amount of computational work (per grid point) needed to solve the sets of algebraic equations resulting from the application of finite-difference approximations to any given order of truncation error.

For the current problem, there are two clear, major disadvantages with the Cartesian approach we outline in this section. The first is that the coordinates do *not* conform to the inner boundaries ("holes") of the problem domain. This means that the formulation of accurate differenced versions of the boundary conditions is considerably more involved here than in the other two approaches described in this paper. Second, because we use a *uniform* Cartesian grid (*constant* mesh increment, h, in each of the coordinate directions), the combination of (1) the need to resolve steep gradients near the holes and (2) limitations on our computational resources (memory and time), places a severe restriction on the radius at which the outer edge of the computational domain is located. In practice this means that we must impose the asymptotic condition (7) in a regime where the neglected terms in the multipole expansion are still significant. These shortcomings are apparent in the numerical results discussed in Sec. IV and we make some brief remarks about potential remedies in Sec. V.

In Cartesian coordinates, Eqs. (3), (5), and (7), which we solve numerically, are

$$\frac{\partial^2\psi}{\partial x^2}+\frac{\partial^2\psi}{\partial y^2}+\frac{\partial^2\psi}{\partial z^2}=-\frac{1}{8}\psi^{-7}\bar{A}^2, \tag{23}$$

$$n^x_\alpha\frac{\partial\psi}{\partial x}+n^y_\alpha\frac{\partial\psi}{\partial y}+n^z_\alpha\frac{\partial\psi}{\partial z}=-\left.\frac{\psi}{2r_\alpha}\right|_{B_\alpha}, \tag{24}$$

$$x\frac{\partial\psi}{\partial x}+y\frac{\partial\psi}{\partial y}+z\frac{\partial\psi}{\partial z}=\frac{1-\psi}{r}, \tag{25}$$

where

$$\bar{A}^2\equiv\bar{A}_{ij}\bar{A}^{ij}, \tag{26}$$

$$r=\sqrt{x^2+y^2+z^2}, \tag{27}$$

$$r_\alpha=\sqrt{(x-x_\alpha)^2+(y-y_\alpha)^2+(z-z_\alpha)^2}, \qquad \alpha=1,2, \tag{28}$$

$\mathbf{n}_\alpha=(n^x_\alpha,n^y_\alpha,n^z_\alpha)$ are the unit normals to the holes, and the "centers" of the holes are located at $\mathbf{C}_\alpha=(x_\alpha,y_\alpha,z_\alpha)$. Equation (24) holds at the hole surfaces and Eq. (25) is imposed at the outer boundary. The nonlinear Hamiltonian constraint is solved iteratively using a linearization which, given an approximate solution ψ_0, determines the new iterate ψ:

$$\frac{\partial^2\psi}{\partial x^2}+\frac{\partial^2\psi}{\partial y^2}+\frac{\partial^2\psi}{\partial z^2}-\frac{7}{8}\bar{A}^2\psi_0^{-8}\,\psi=-\bar{A}^2\psi_0^{-7}. \tag{29}$$

The computational domain we use is a subset of a uniform, cubical lattice centered at $(0,0,0)$ and having $n+1$ grid-points on an edge:

$$\{(ih,jh,kh)\}, \qquad i,j,k=-\frac{n}{2},-\frac{n}{2}+1,\ldots,\frac{n}{2}-1,\frac{n}{2}, \tag{30}$$

where h is the (unique) discretization scale. As a matter of convenience, we will refer to *any* point with coordinates of the form (ih,jh,kh), with i, j, k integers, as a lattice point, even though it may not be contained in the actual computational domain. One of the key features of the Cartesian approach is that points of the lattice (30) are used to approximate the inner boundaries (i.e., the "holes") of the solution domain. Figure 2 schematically illustrates a typical computational domain which might be used for the case of a computation involving a single hole in two dimensions. Define two lattice points to be *nearest neighbors* of each other if they are separated by precisely one unit in any *single* coordinate direction. Thus, any lattice point in two or three dimensions has four or six nearest neighbors, respectively. A "surface" in the lattice is *closed* if it separates the lattice points into two disjoint sets such that no member of one set is

a nearest neighbor of a member of the other set. In general then, the boundary points representing a hole (such as those marked with a • in the figure) are chosen so that (1) each set of boundary points is closed and (2) the points are as close as possible to the true location of the continuum inner boundary.

In addition to the inner boundary points, the computational domain contains *interior* points (those marked with a + in the figure) and outer boundary points (filled boxes). We further categorize any point on a boundary as a *single-edge*, *double-edge*, or *triple-edge* boundary point according to whether the point has one, two, or three nearest-neighbors, respectively, which lie *outside* of the discrete domain. For example, in Fig. 2, the four corner points are double-edge boundary points, and the remaining outer boundary points are single-edge. Similarly, there are six double-edge *inner* boundary points in the figure, including the point enclosed by the doubled-diamond. As we shall now discuss, this substantial variety in the types of points in the computational domain results in a proliferation of specific difference equations which must be generated in order to produce a reasonably accurate solution.

Our finite-difference analogues of the system (29), (24), and (25) are generated using standard $O(h^2)$ centered, forward, and backward approximations to first and second derivatives. However, as discussed below, and in contrast to the previously described scheme based on Čadež coordinates, we have *not* implemented a scheme with true $O(h^2)$ truncation error; rather we anticipate only $O(h)$ convergence in the limit $h \to 0$ and possibly indeterminate convergence behavior at practical resolutions.

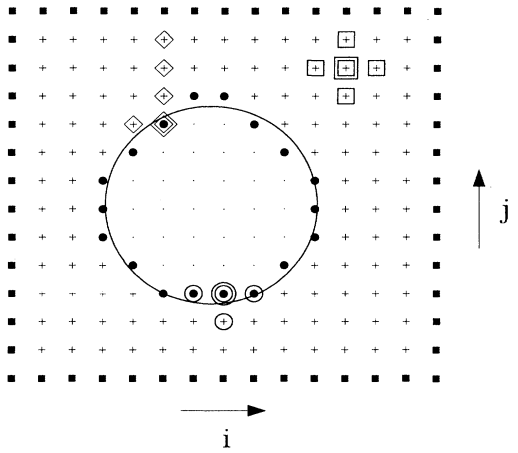

FIG. 2. Schematic representation of the computational domain for a hypothetical, 2D, single-hole Cartesian calculation. i and j are lattice indices. Plus signs denote interior points; filled circles and squares mark inner and outer boundary points respectively. Points marked with a dot (in the interior of the hole) are not used in the computation. The three groupings of larger symbols represent three distinct finite-difference *stencils*, each of which is "centered" at the point surrounded by a doubled symbol. See text for further explanation.

Adopting the usual finite-difference notation $f(ih, jh, kh) \equiv f_{i,j,k}$, we employ the following formulas for the x derivatives:

$$\frac{\partial\psi}{\partial x}(ih,jh,kh) \equiv \frac{\partial\psi}{\partial x}_{i,j,k}$$

$$= \frac{\psi_{i+1,j,k} - \psi_{i-1,j,k}}{2h} + O(h^2) \tag{31}$$

$$= \frac{-\psi_{i+2,j,k} + 4\psi_{i+1,j,k} - 3\psi_{i,j,k}}{2h} + O(h^2) \tag{32}$$

$$= \frac{3\psi_{i,j,k} - 4\psi_{i-1,j,k} + 3\psi_{i-2,j,k}}{2h} + O(h^2), \tag{33}$$

$$\frac{\partial^2\psi}{\partial x^2}(ih,jh,kh) \equiv \frac{\partial^2\psi}{\partial x^2}_{i,j,k}$$

$$= \frac{\psi_{i+1,j,k} - 2\psi_{i,j,k} + \psi_{i-1,j,k}}{h^2} + O(h^2) \tag{34}$$

$$= \frac{-\psi_{i+3,j,k} + 4\psi_{i+2,j,k} - 5\psi_{i+1,j,k} + 2\psi_{i,j,k}}{h^2} + O(h^2) \tag{35}$$

$$= \frac{2\psi_{i,j,k} - 5\psi_{i-1,j,k} + 4\psi_{i-2,j,k} - \psi_{i-3,j,k}}{h^2} + O(h^2), \tag{36}$$

and the obvious counterparts for the y and z derivatives. As is often the case in finite-difference work, it is convenient to describe the derivation of our discrete equations in terms of *stencils*. The stencil associated with any given finite-difference expression applied at some generic lattice point (ih, jh, kh) is simply the set of points (or neighborhood) explicitly referenced in that expression. Again, for illustrative purposes, Fig. 2 displays examples of three distinct stencils for the two-dimensional case. Each stencil is represented as a grouping of large-sized symbols and each stencil is to be considered *centered* at the lattice point surrounded by a doubled symbol. For each distinct stencil we derive a separate difference equation based on a discretization of the interior equation (29) and, where appropriate, one of the boundary conditions (24) or (25). In order to gain some sense of how this process is carried out for the 3D, two black-hole case, it is instructive to consider the derivation of 2D difference

equations associated with the three stencils depicted in Fig. 2.

We first consider the stencil represented by boxes in Fig. 2. Using (34) and the analogous formula for the y derivative in (29) and ignoring any z dependence, we obtain the difference expression

$$\frac{\psi_{i+1,j}+\psi_{i-1,j}+\psi_{i,j+1}+\psi_{i,j-1}-4\psi_{i,j}}{h^2} - \frac{7}{8}\left[\bar{A}^2\psi_0^{-8}\right]_{i,j}\psi_{i,j} = -\left[\bar{A}^2\psi_0^{-7}\right]_{i,j}, \quad (37)$$

which may also be applied at any other grid point marked with a +.

Now consider the stencil composed of circles which is centered at the double-circled point. In this case, we use centered-differenced versions of both the interior equation (29) and the inner boundary condition (24). Thus, in addition to (37) we have

$$n^x_{i,j}\left[\frac{\psi_{i+1,j}-\psi_{i-1,j}}{2h}\right] + n^y_{i,j}\left[\frac{\psi_{i,j+1}-\psi_{i,j-1}}{2h}\right] = -\frac{\psi_{i,j}}{2r_{i,j}}. \quad (38)$$

Note that although we have used "second-order" differences to generate this last expression, it is, for a general inner boundary point, only a *first-order* accurate version of the inner boundary condition since the boundary point will, as shown in the figure, generally lie a distance $O(h)$ from the $r = r_\alpha$ surface. Second-order accurate formulas *could* be generated using Taylor series expansion and the governing differential equations, but we have not done so. Now, (37) and (38) both involve the value $\psi_{i,j+1}$, which is defined on a lattice point lying outside the computational domain. Therefore, we solve (38) for $\psi_{i,j+1}$, and substitute the result in (37), yielding an expression involving only the points of the stencil:

$$h^{-2}\left(\left[1-\frac{n^x}{n^y}\right]_{i,j}\psi_{i+1,j} + \left[1+\frac{n^x}{n^y}\right]_{i,j}\psi_{i-1,j} + 2\psi_{i,j-1} - \left[4+\frac{h}{rn^y}\right]_{i,j}\psi_{i,j}\right) - \frac{7}{8}\left[\bar{A}^2\psi_0^{-8}\right]_{i,j}\psi_{i,j} = -\left[\bar{A}^2\psi_0^{-7}\right]_{i,j}. \quad (39)$$

The stencil marked by diamonds in Fig. 2 is centered on a double-edge boundary point. In this case, application of centered difference formulas to the interior and boundary equations results in references to *two* points which lie outside of the computational domain. In order to derive a *single* equation for the center point we employ forward differencing in the y direction, and centered differencing in the x direction to get

$$\frac{\psi_{i+1,j}+\psi_{i-1,j}-\psi_{i,j+3}+4\psi_{i,j+2}-5\psi_{i,j+1}}{h^2} - \frac{7}{8}\left(\bar{A}^2\psi_0^{-8}\right)_{i,j}\psi_{i,j} = -\left[\bar{A}^2\psi_0^{-7}\right]_{i,j} \quad (40)$$

and

$$n^x_{i,j}\left[\frac{\psi_{i+1,j}-\psi_{i-1,j}}{2h}\right] + n^y_{i,j}\left[\frac{-\psi_{i,j+2}+4\psi_{i,j+1}-3\psi_{i,j}}{2h}\right] = -\frac{\psi_{i,j}}{2r_{i,j}}. \quad (41)$$

As before, solution of the discrete boundary condition for the value $\psi_{i+1,j}$, followed by substitution of the result into the differenced interior equation, yields a single equation involving only the stencil unknowns:

$$h^{-2}\left(2\psi_{i-1,j} - \psi_{i,j+3} + \left[4-\frac{n^y}{n^x}\right]_{i,j}\psi_{i,j+2} + \left[4\frac{n^y}{n^x}-5\right]_{i,j}\psi_{i,j+1} - \left[3\frac{n^y}{n^x}-\frac{h}{rn^x}\right]_{i,j}\psi_{i,j}\right) - \frac{7}{8}\left[\bar{A}^2\psi_0^{-8}\right]_{i,j}\psi_{i,j} = -\left[\bar{A}^2\psi_0^{-7}\right]_{i,j}. \quad (42)$$

As a last example of the derivation of our difference equations in Cartesian coordinates, we consider yet again the case of a stencil centered on a boundary point of a hole, but this time for the 3D case. Let the center point have coordinates (ih, jh, kh) and assume that of the point's six nearest neighbors, the three with coordinates $((i-1)h, jh, kh)$, $(ih, (j-1)h, kh)$, and $(ih, jh, (k-1)h)$ lie outside the numerical domain. Then, by definition, (ih, jh, kh) is a triple-edge boundary point. In such a case, we use forward differences in two of the coordinate directions, and centered differences in the other. Now, as we will discuss shortly, the complete set of difference equations is solved using a line-relaxation method in which *blocks* of unknowns, such as $\psi_{i,j,k}$, $i = -n/2 \cdots n/2$ with j and k fixed, are updated ("relaxed") simultaneously. We will refer to the coordinate direction along which a block of unknowns extends as the *scanning* direction. Then, at a triple-edge boundary point, we always forward or backward difference in the scanning direction. To determine the type of differencing to be applied along the other two directions, we examine the components of the normal—the direction having the *smallest* component is the direction in which we use centered differences. In the current example, assume we are scanning in the x direction and that $|n^z_{i,j,k}| < |n^y_{i,j,k}|$, then we use forward differences in the x and y directions and centered differences in the z direction to get the following discrete forms of the Hamiltonian constraint and inner boundary condition:

$$h^{-2}\,[-\psi_{i+3,j,k} + 4\psi_{i+2,j,k} - 5\psi_{i+1,j,k} - \psi_{i,j+3,k} + 4\psi_{i,j+2,k} - 5\psi_{i,j+1,k} + \psi_{i,j,k+1} + \psi_{i,j,k-1} + 2\psi_{i,j,k}] - \frac{7}{8}\left[\bar{A}^2\psi_0^{-8}\right]_{i,j}\psi_{i,j} = -\left[\bar{A}^2\,\psi_0^{-7}\right]_{i,j}, \quad (43)$$

$$n^x_{i,j,k}\left[\frac{-\psi_{i+2,j,k} + 4\psi_{i+1,j,k} - 3\psi_{i,j,k}}{2h}\right] + n^y_{i,j,k}\left[\frac{-\psi_{i,j+2,k} + 4\psi_{i,j+1,k} - 3\psi_{i,j,k}}{2h}\right] + n^z_{i,j,k}\left[\frac{\psi_{i,j,k+1} - \psi_{i,j,k-1}}{2h}\right] = -\frac{\psi_{i,j,k}}{2r_{i,j,k}}. \quad (44)$$

Solving (44) for $\psi_{i,j,k-1}$ and substituting in (43) we get

$$h^{-2}\Bigg(- \psi_{i+3,j,k} + \left[4 - \frac{n^x}{n^z}\right]_{i,j,k}\psi_{i+2,j,k} + \left[4\frac{n^x}{n^z} - 5\right]_{i,j,k}\psi_{i+1,j,k} - \psi_{i,j+3,k} + \left[4 - \frac{n^y}{n^z}\right]_{i,j,k}\psi_{i,j+2,k} + \left[4\frac{n^y}{n^z} - 5\right]_{i,j,k}\psi_{i,j+1,k} + 2\psi_{i,j,k+1} + \left[2 + \frac{h}{rn^z} - 3\frac{n^x}{n^z} + 3\frac{n^y}{n^z}\right]_{i,j,k}\psi_{i,j,k}\Bigg) - \frac{7}{8}\left[\bar{A}^2\psi_0^{-8}\right]_{i,j,k}\psi_{i,j,k} = -\left[\bar{A}^2\,\psi_0^{-7}\right]_{i,j,k}. \quad (45)$$

Clearly, there are seven other distinct stencils for inner triple-edge boundaries in three dimensions, all of which can be readily obtained from (45) by suitable permutations of the i, j, and k indices.

At this point, the procedure we use to generate our difference equations should be reasonably clear. Altogether, including the various single-, double-, and triple-edge boundary cases, we use 77 distinct stencils in the code.

The finite-difference discretization of (29), (24), and (25) we have outlined above produces a large, sparse set of linear equations which, as mentioned previously, is solved using an iterative, line-relaxation technique. The "kernel" of the algorithm, a single line-relaxation sweep, can be most clearly defined and understood if we momentarily ignore boundary conditions and focus on the solution of the differenced form of (29):

$$h^{-2}\left(\psi_{i+1,j,k} + \psi_{i-1,j,k} + \psi_{i,j+1,k} + \psi_{i,j-1,k} + \psi_{i,j,k+1} + \psi_{i,j,k-1} - 6\psi_{i,j,k}\right) - \frac{7}{8}\left[\bar{A}^2\psi_0^{-8}\right]_{i,j,k}\psi_{i,j,k} = -\left[\bar{A}^2\,\psi_0^{-7}\right]_{i,j,k}. \quad (46)$$

Now, let $\psi^{(m)}_{i,j,k}$ denote the values of the stored grid function after the mth iteration of the solution process. Then, the equations

$$h^{-2}\left(\psi^{(m+1)}_{i+1,j,k} - 2\psi^{(m+1)}_{i,j,k} + \psi^{(m+1)}_{i-1,j,k}\right) - \frac{7}{8}\left[\bar{A}^2\psi^{-8}\right]^{(m)}_{i,j,k}\psi^{(m+1)}_{i,j,k} = -h^{-2}\left(\psi^{(m)}_{i,j+1,k} + \psi^{(m)}_{i,j-1,k} + \psi^{(m)}_{i,j,k+1} + \psi^{(m)}_{i,j,k-1} - 4\psi^{(m)}_{i,j,k}\right) - \left[\bar{A}^2\psi^{-7}\right]^{(m)}_{i,j,k} \quad (47)$$

define a *line-Gauss-Seidel* (LGS) iteration for the system (46). For fixed j and k, (47) is a linear tridiagonal system for the $n+1$ unknowns $\psi^{(m+1)}_{i,j,k}, i = -n/2 \cdots n/2$. A complete *relaxation sweep* consists of the solution of $(n+1)^2$ such tridiagonal systems, one for each pairing of j and k—after such a sweep each unknown has been updated exactly one time. We refer to the iteration defined by (47) as x-LGS since the lines of unknowns which are simultaneously updated extend along the x direction. Clearly, we can also define y-LGS and z-LGS iterations.

Gauss-Seidel relaxation generally has a notoriously slow convergence rate, particularly in the limit $h \to 0$. In order to speed convergence, it is usually helpful to employ the technique of *overrelaxation*. For example, associated with the x-LGS iteration (47) is the x-LSOR (line successive overrelaxation) iteration:

$$\psi^{(m+1)}_{i,j,k} = \omega\tilde{\psi}^{(m+1)}_{i,j,k} + (1-\omega)\,\psi^{(m)}_{i,j,k}, \quad (48)$$

where $\tilde{\psi}^{(m+1)}_{i,j,k}$ satisfies the Gauss-Seidel equations (47), and ω is the overrelaxation parameter which generally must satisfy $1 \le \omega < 2$. Although our algorithm incorporates this strategy, with an h-dependent, empirically determined ω, we also use another, somewhat *ad hoc*, technique which basically amounts to an additional overrelaxation applied on a pointwise basis. Again, assuming that we are scanning in the x direction, rather than solving (47), we solve

$$h^{-2}\left(\psi^{(m+1)}_{i+1,j,k} - 4\psi^{(m+1)}_{i,j,k} + \psi^{(m+1)}_{i-1,j,k}\right) - \frac{7}{8}\left[\bar{A}^2\psi^{-8}\right]^{(m)}_{i,j,k}\psi^{(m+1)}_{i,j,k}$$

$$= -h^{-2}\left(\psi^{(m)}_{i,j+1,k} + \psi^{(m)}_{i,j-1,k} + \psi^{(m)}_{i,j,k+1} + \psi^{(m)}_{i,j,k-1} - 2\psi^{(m)}_{i,j,k}\right) - \left[\bar{A}^2\psi^{-7}\right]^{(m)}_{i,j,k}. \quad (49)$$

Together, equations (47) and (49) define the core of what we call an x-LSOR sweep. Where necessary, boundary equations are simultaneously solved with the interior equations [such as (47)], but boundary values are never overrelaxed.

Briefly then, our complete iterative procedure for solving the Hamiltonian constraint proceeds as follows. We perform x-LSOR, y-LSOR, and z-LSOR sweeps in succession until

$$\left\|\psi^{(m+1)}_{i,j,k} - \psi^{(m)}_{i,j,k}\right\|_2 < \epsilon, \quad (50)$$

for some convergence parameter, ϵ, typically 1×10^{-6}. Each d-LSOR sweep ($d = x, y$ or z) requires the solution of $(n+1)^2$ linear systems in $n+1$ unknowns. Each linear system is either (1) *tridiagonal*, a situation which occurs whenever the discrete equations involve only centered differences in the d direction or (2) *7 diagonal*, if the equations involve forward or backward differences in the d-direction. The tridiagonal systems are solved using a tridiagonal solver which has been optimized for the particular machine architectures (Cray Y/MP, Cray 2) on which the code is run, while the 7 diagonal systems are solved using a biconjugate-gradient method. In both cases, the linear system can be solved using $O(n)$ operations, so a complete d-LSOR sweep requires $O(n^3)$ computational work. Empirically, we usually obtain convergence with $O(n)$ sweeps; this represents the optimal asymptotic performance which can be expected for an LSOR method. Thus, our algorithm requires $O(N^{4/3})$ operations to compute a solution on a mesh containing $N \approx n^3$ unknowns. We note that for large N this implies significantly poorer performance than should be possible with a multigrid technique.

C. The multiquadric approach

The multiquadric (MQ) approximation scheme was first used by Hardy in 1968 for two-dimensional (2D) surface interpolation of geographical data points, measured at arbitrary locations [9]. Since that time, there have been a number of significant theoretical [17] and practical [18] developments in its use. Kansa [19] was the first to apply the method to the solution of partial differential equations, and his techniques are basically those followed here.

The use of MQ in numerical relativity has been described in two previous papers [20, 21]. In Ref. [20] a number of numerical experiments were performed to test the feasibility of the method. Single black-hole initial data sets in 3D Cartesian coordinates were constructed and MQ was found to be accurate and very easy to implement. In Ref. [21], a brief description was given of the extension of that work to the construction of 3D initial-data sets for two black holes in the case of Misner data [22]. A short discussion of the numerical difficulties encountered and some possible remedies was also presented. Here, we extend those previous works further in order to construct general 3D two-black-hole initial data, once again in a Cartesian coordinate system.

References [20, 21] indicated that a straightforward application of MQ to the solution of the Hamiltonian constraint for ψ produces poor results due to the asymptotically flat nature of the conformal factor (for flat or mild gradients, MQ is noisy and inaccurate). Substantially more accurate results were obtained by transforming to a new variable, Φ, whose growth is *unbounded* with distance—such behavior is better represented by the MQ basis function [23]. Based on the single-black-hole and Misner data experiments, Φ is given by

$$\psi = 1 + \left[\left(\frac{a_1}{r_1}\right)^3 + \left(\frac{a_2}{r_2}\right)^3 + \left(\frac{a_1 a_2}{r_1 r_2}\right)^{3/2}\right]\Phi = 1 + \mathcal{A}\Phi. \quad (51)$$

In the above, if $\mathbf{C}_\alpha$ are the coordinate positions of the centers of holes $\alpha = 1, 2$, then $r_\alpha^2 = \delta_{ij}\Delta x^i_\alpha \Delta x^j_\alpha$, where $\Delta\mathbf{x}_\alpha = \mathbf{x} - \mathbf{C}_\alpha$, a_α are the radii of the holes and δ_{ij} is the Kronecker δ function. Then, Eq. (3) is transformed to become

$$\mathcal{A}\bar{\nabla}^2\Phi - 6\left\{\frac{a_1^3}{r_1^5}\left[1 + \frac{1}{2}\left(\frac{r_1 a_2}{r_2 a_1}\right)^{3/2}\right]\Delta x^i_1\bar{\nabla}_i\Phi + \frac{a_2^3}{r_2^5}\left[1 + \frac{1}{2}\left(\frac{r_2 a_1}{r_1 a_2}\right)^{3/2}\right]\Delta x^i_2\bar{\nabla}_i\Phi\right\}$$

$$+\left\{6\left[\frac{a_1^3}{r_1^5} + \frac{a_2^3}{r_2^5}\right] + \frac{3}{4}\left(\frac{a_1 a_2}{r_1 r_2}\right)^{3/2}\left[\frac{1}{r_1} + \frac{1}{r_2} + \frac{6\mathcal{D}}{r_1^2 r_2^2}\right]\right\}\Phi = -\frac{1}{8}\bar{A}_{ij}\bar{A}^{ij}\left[1 + \mathcal{A}\Phi\right]^{-7}, \quad (52)$$

where $\bar{\nabla}^2$ and $\bar{\nabla}_i$ are the flat space Cartesian Laplacian and grad operators respectively, and $\mathcal{D} = \delta_{ij}\Delta x^i_1 \Delta x^j_2$. The boundary conditions also need to be transformed. On the spherical outer boundary of radius $r_{\rm outer}$, expression (7) is written as

$$\mathcal{A}x^i\bar{\nabla}_i\Phi + \left[\left(\frac{a_1}{r_1}\right)^3\left(1-\frac{3\mathcal{D}_1}{r_1^2}\right)+\left(\frac{a_2}{r_2}\right)^3\left(1-\frac{3\mathcal{D}_2}{r_2^2}\right) + \left(\frac{a_1a_2}{r_1r_2}\right)^{3/2}\left(1-\frac{3\mathcal{D}_1}{2r_1^2}-\frac{3\mathcal{D}_2}{2r_2^2}\right)\right]\Phi = 0, \tag{53}$$

holding at $\delta_{ij}x^ix^j = r_{\text{outer}}^2$, where $\mathcal{D}_\alpha = \delta_{ij}x^i\Delta x_\alpha^j$. The boundary condition (5) at the throat of hole 2, in terms of Φ, is written as

$$\mathcal{A}\Delta x_2^i\bar{\nabla}_i\Phi - \left[\frac{5}{2}+\left(\frac{a_1}{r_1}\right)^3\left(\frac{3\mathcal{D}}{r_1^2}-\frac{1}{2}\right) + \frac{1}{2}\left(\frac{a_1}{r_1}\right)^{3/2}\left(1+\frac{3\mathcal{D}}{2r_1^2}\right)\right]\Phi = -\frac{1}{2}, \tag{54}$$

holding at $\delta_{ij}\Delta x_2^i\Delta x_2^j = a_2^2$. A similar expression can be written for the boundary condition at the throat of hole 1.

Although the resulting system is more cumbersome than the original one, nevertheless it is still a simple procedure to solve it using the MQ method. To begin, the function Φ is approximated as a linear sum of MQ basis functions plus an appended constant [19, 23]

$$\Phi = c_1 + \sum_{q=2}^{N} c_q\tilde{g}_q, \tag{55}$$

where c_q are the expansion coefficients to be determined, N is the total number of data points used and $\tilde{g}_q$ is given by $\tilde{g}_q = g_q - g_1$, with g_q the MQ radial basis function

$$g_q = [(x-x_q)^2 + (y-y_q)^2 + (z-z_q)^2 + s_q^2]^{1/2}. \tag{56}$$

In Eq. (56), following Kansa [19], the quantity s_q^2 is given by

$$s_q^2 = s_{\min}^2\left(\frac{s_{\max}^2}{s_{\min}^2}\right)^{(q-1)/(N-1)}, \tag{57}$$

where $s_{\min/\max}$ are *arbitrary* input parameters. Although arbitrary, the actual values of $s_{\min/\max}$ do affect the accuracy of the solution obtained (see, e.g., Ref. [20]) and so this can be a difficulty in the practical use of MQ. Some experimentation is required; however, Ref. [20] indicates that, in general, the ratio $s_{\max}/s_{\min}$ should be as large as possible, consistent with solutions that are not obviously incorrect (e.g., wild oscillations). For all the MQ computations described in this paper we set typical values of $s_{\min} = 1$ and $s_{\max} = 4000$.

It should be noted that many other choices of s_q^2 are possible [18]. Various schemes for choosing expressions for s_q^2 have been discussed in Refs. [9, 18], but most of these schemes are understood heuristically at best, and are generally tuned on the basis of empirical studies. Expression (57) appears to work well since it produces a diverse range of basis function shapes, which helps in approximating a wide variety of surfaces.

While the MQ approach allows the positions of the N data points (x_q, y_q, z_q) to be arbitrary, it is prudent to have a dense distribution of points in those regions of the computational domain where the functions to be evaluated are expected to vary most rapidly. For the problem at hand this is obviously around the throats of the two black holes. Figure 3 shows the distribution of data points for the high resolution A1B8 configuration (discussed in the next section). On the left-hand side all $N = 1994$ points are shown in projection. The right-hand side shows the same projections for the region near the black holes. These points have been distributed so as to lie on two sets of concentric spherical surfaces with radii increasing geometrically (by a factor of ≈ 1.1) from the center of each hole. The outer boundary points have been placed on a spherical surface satisfying $r_{\text{outer}} = 350$ for this particular case, and the radii of the two holes is $a_1 = a_2 = 1$. Note that no data points lie inside the holes, i.e. within the regions defined by $\delta_{ij}\Delta x_\alpha^i\Delta x_\alpha^j < a_\alpha^2$.

Now, given the expansion (55), it is a simple matter to construct first, second, and higher derivative approximations of Φ, for example,

$$\frac{\partial\Phi}{\partial x} = \sum_{q=2}^{N} c_q\frac{\partial\tilde{g}_q}{\partial x} = \sum_{q=2}^{N} c_q\left[\frac{x-x_q}{g_q}-\frac{x-x_1}{g_1}\right] \tag{58}$$

and

$$\frac{\partial^2\Phi}{\partial x^2} = \sum_{q=2}^{N} c_q\frac{\partial^2\tilde{g}_q}{\partial x^2} = \sum_{q=2}^{N} c_q\left[\frac{1}{g_q}-\frac{1}{g_1}-\frac{(x-x_q)^2}{g_q^3} + \frac{(x-x_1)^2}{g_1^3}\right], \tag{59}$$

which, along with (55), can be substituted into Eqs. (52)–(54). Since Eq. (52) is nonlinear, however, global linearization is required first, similar to Eq. (29) of Sec. III B. Once the substitutions have been made the result is a system of N linear algebraic equations for the coefficients c_q. This system can be written in the matrix form

$$\mathbf{Sc} = \mathbf{b}, \tag{60}$$

where $\mathbf{c} = (c_1, c_2, \ldots, c_N)^{\mathrm{T}}$ and where the entries of $\mathbf{S}$ and $\mathbf{b}$ are given by

$$S_{p1} = \frac{6}{\mathcal{A}}\left[\frac{a_1^3}{r_1^5}+\frac{a_2^3}{r_2^5}\right] + \frac{3}{4\mathcal{A}}\left(\frac{a_1a_2}{r_1^2r_2^2}\right)^{3/2}\left[\frac{1}{r_1^2}+\frac{1}{r_2^2}+\frac{6\mathcal{D}}{r_1^2r_2^2}\right] - \frac{7}{8}\bar{A}_{ij}\bar{A}^{ij}[1+\mathcal{A}\Phi_0]^{-8},$$

$$S_{pq} = \tilde{g}_qS_{p1} + 3\left[\frac{1}{g_q}-\frac{1}{g_1}\right] - \left[\frac{\delta_{ij}(x_p^i-x_q^i)(x_p^j-x_q^j)}{g_q^3}-\frac{\delta_{ij}(x_p^i-x_1^i)(x_p^j-x_1^j)}{g_1^3}\right] - \frac{6}{\mathcal{A}}\left\{\frac{a_1^3}{r_1^5}\left(1+\frac{1}{2}\left(\frac{a_2r_1}{a_1r_2}\right)^{3/2}\right)[\mathcal{F}_{1(pq)}-\mathcal{F}_{1(p1)}] + \frac{a_2^3}{r_2^5}\left(1+\frac{1}{2}\left(\frac{a_1r_2}{a_2r_1}\right)^{3/2}\right)[\mathcal{F}_{2(pq)}-\mathcal{F}_{2(p1)}]\right\},$$

$$b_p = -\frac{1}{8}\bar{A}_{ij}\bar{A}^{ij}[1+\mathcal{A}\Phi_0]^{-7}\left(\frac{1}{\mathcal{A}}+\frac{7\Phi_0}{1+\mathcal{A}\Phi_0}\right),$$

$$\mathcal{F}_{\alpha(pq)} = \frac{\delta_{ij}\Delta x^i_\alpha (x^j_p - x^j_q)}{g_q}$$

if the data point (x_p, y_p, z_p) lies within the interior of the computational domain, by

$$S_{p1} = \left(\frac{a_1}{r_1}\right)^3\left(1-\frac{3\mathcal{D}_1}{r_2^2}\right)^3 + \left(\frac{a_2}{r_2}\right)\left(1-\frac{3\mathcal{D}_2}{r_2^2}\right) + \left(\frac{a_1 a_2}{r_1 r_2}\right)^{3/2}\left(1-\frac{3\mathcal{D}_1}{2r_1^2}-\frac{3\mathcal{D}_2}{2r_2^2}\right),$$

$$S_{pq} = \tilde{g}_q S_{p1} + \mathcal{A}\left[\frac{\delta_{ij}x^i_p(x^j_p - x^j_q)}{g_q} - \frac{\delta_{ij}x^i_p(x^j_p - x^j_1)}{g_1}\right],$$

$$b_p = 0$$

if (x_p, y_p, z_p) lies on the boundary at r_{outer}, and by

$$S_{p1} = -\left[\frac{5}{2}+\left(\frac{a_1}{r_1}\right)^3\left(\frac{3\mathcal{D}}{r_1^2}-\frac{1}{2}\right) + \frac{1}{2}\left(\frac{a_1 a_2}{r_1 r_2}\right)^{3/2}\left(1+\frac{3\mathcal{D}}{2r_1^2}\right)\right],$$

$$S_{pq} = \tilde{g}_q S_{p1} + \mathcal{A}\left[\mathcal{F}_{2(pq)} + \mathcal{F}_{2(p1)}\right],$$

$$b_p = -\frac{1}{2}$$

if (x_p, y_p, z_p) lies on the throat of hole 2 (similar expressions hold for points lying on the throat of hole 1). In the above all quantities that are not specifically labeled with an index p or q are evaluated in terms of the data point (x_p, y_p, z_p).

Kansa [19] and Dubal [20], among others, have dis-

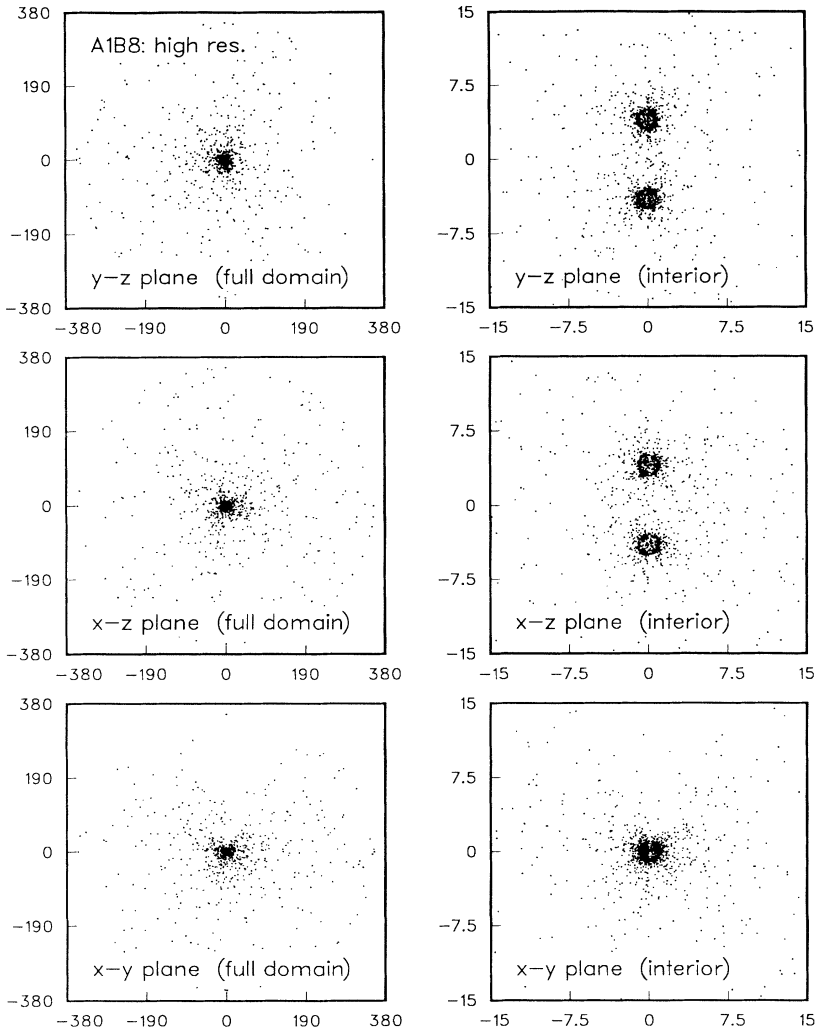

FIG. 3. Typical distribution of data points for a multiquadrics computation. Each panel on the left-hand side is a projection of all N data points onto a plane passing through the origin. Panels on the right show details of the point distribution near the holes.

cussed the highly ill-conditioned nature of the system (60). In general, $\mathbf{S}$ is a *full* $N \times N$ matrix with a condition number $\sim 10^{20}$ or higher. The solution of (60) is not amenable to straightforward LU decomposition—standard iterative and direct methods will not work due to roundoff error. As shown in Ref. [20], however, it can be solved successfully using the method of *singular-value decomposition* (SVD) [24, 25] with single-precision FORTRAN arithmetic on a Cray Y-MP8/864 (64-bit word representation). The routine SVDCMP described in Ref. [24] worked well for this problem. The quantity Φ_0 is obtained via the expansion (55) using previously computed values of c_q (or an initial guess), and is updated using fixed-point iteration of (60) (see Ref. [20]). In the majority of cases convergence of Φ is rapid, taking less than ten iterations to achieve a maximum relative difference of $< 1 \times 10^{-6}$ between adjacent iterated values of Φ. We also use iterative refinement [24] to recover some of the lost significant figures in the solution of (60). Unfortunately, the SVD algorithm is expensive since it has a high operation count at $O(N^3)$, although for many problems N can be considerably smaller in the case of MQ than for finite-difference methods, for a given level of accuracy.

IV. RESULTS AND COMPARISON OF METHODS

A. Methodology

In this section, we assess and compare the relative performance of the three algorithms described above by considering the solution of the Hamiltonian constraint for several initial configurations describing two black holes. The basic methodology we adopt in our analysis is the straightforward technique of *convergence testing*—for any given physical problem and specific solution technique we generate numerical results at several different *resolutions* (different basic scales of discretization h for the finite-difference methods, or number N of basis functions for the MQ). From these *convergence series* we can then estimate, in the ideal case, (1) the actual level of error, at a given resolution, in any given solution, and (2) the rate of convergence of the numerical solution to the continuum solution, again at some specific resolution. This approach was adopted in a previous comparison (Choptuik *et al.* [10]) of different numerical techniques which had been designed for the solution of a particular problem in numerical relativity. The point of this approach is that, at least for finite difference codes, quantities such as the level of error and convergence rate should be *intrinsically* (i.e., without reference to an analytic solution or a previously computed numerical solution) assessable. However, the error analysis of the basic numerical methods employed in [10] was expedited by the availability of high-accuracy numerical results generated from the application of Richardson-extrapolation techniques to the "raw" output of one of the methods. In the current case as well, the convergence behavior of one of the methods—the Čadež scheme—is such that the output from the algorithm is amenable to Richardson extrapolation. Both theoretical and empirical evidence support our confidence that these extrapolated values are sufficiently accurate to be considered exact for the purpose of assessing the errors and convergence rates of the "raw" output of the three different methods.

B. Model parameters

We have considered five different models in our comparison of the three methods. As illustrated in Table I, each model is characterized by a considerable number of parameters. Recall from Sec. III A Eq. (9) that α is the dimensionless ratio of the radii of the two holes, while β is the spatial separation of the holes in units of the radius of the first hole, a_1. The three-vectors $\mathbf{P}_1$, $\mathbf{P}_2$, $\mathbf{S}_1$ and $\mathbf{S}_2$ can be associated, roughly speaking, with the linear momenta and spins of the two holes—the identification becomes precise only in the limit of large separation of the holes. The parameter $r_{\rm outer}$ differs from the other six in that it has no physical significance—rather, it is the approximate outer radius of the computational domain [the radius at which the Robin boundary condition (7) is imposed] used in the corresponding Čadež calculations which, in turn, were used to generate the reference results. Note that in terms of the six *physical* parameters there are only three distinct models—A2B8TS (TS since the initial data for this case generates a time-symmetric spacetime), A1B8 and A2B8. Models A1B8NR (NR for near) and A2B8NR differ from their non-NR counterparts only in the setting of $r_{\rm outer}$, which, for the NR computations, was chosen to roughly coincide with the outer "radius" of the computational domain used in the Cartesian calculations. For all of the Cartesian computations, this radius was about $14\,a_1$. By generating reference values with a reduced $r_{\rm outer}$, we are able to assess the effect of the smaller computational domain (relative to the other two algorithms) employed in the Cartesian solutions. The point is that imposing the boundary condition (7) at a smaller outer radius, $r'_{\rm outer} < r_{\rm outer}$, does not produce the same solution as that obtained by trun-

TABLE I. Parameters for various two-hole calculations used in the comparison.

Model	α	β	$\mathbf{P}_1/a_1$	$\mathbf{S}_1/a_1^2$	$\mathbf{P}_2/a_1$	$\mathbf{S}_2/a_1^2$	$r_{\rm outer}/a_1$
A2B8TS	2	8	(0,0,0)	(0,0,0)	(0,0,0)	(0,0,0)	730
A1B8	1	8	(14,0,0)	(−280,280,0)	(−14,0,0)	(0,280,280)	350
A1B8NR	1	8	(14,0,0)	(−280,280,0)	(−14,0,0)	(0,280,280)	17
A2B8	2	8	(15,0,0)	(−20,20,0)	(−15,0,0)	(0,20,20)	730
A2B8NR	2	8	(15,0,0)	(−20,20,0)	(−15,0,0)	(0,20,20)	18

cating at $r'_{\rm outer}$ a solution with the boundary condition set at $r_{\rm outer}$.

We ascribe no particular physical significance to the three basic models we consider; the various parameter combinations enumerated in Table I were chosen to produce relatively interesting and illuminating data sets from the numerical viewpoint, which were also germane to the issue of generating initial data for "realistic" black-hole encounters. Thus, based on experience gleaned from axisymmetric computations [3, 26], we chose $\beta = 8$ for the separation parameter in order to produce configurations containing two separate holes (no single, outer apparent horizon or event horizon which envelops both throats), yet where interaction effects are still significant. We include a time-symmetric model providing us with an analytic solution [22], and a useful calibration of our error-assessment. For the models with nonvanishing $\mathbf{P}_\alpha$, each hole has momentum corresponding to relativistic motion. In addition, the total linear momentum of the "configuration" vanishes ($\mathbf{P}_1 + \mathbf{P}_2 = 0$) so as not to degrade the Robin boundary condition (7). The spin vectors $\mathbf{S}_\alpha$ endow the holes in the A1B8/A1B8NR and A2B8/A2B8NR models with what we consider "large" and "moderate" amounts of spin, respectively (the A1B8 holes are almost certainly nearly maximal). The cases with nonvanishing $\mathbf{P}_\alpha$ are "3 dimensional" but, without spin, contain an orbital-plane symmetry. The spin vectors were chosen to explicitly break this remaining symmetry and ensure that the models were truly "generic". Finally, for all models, the coordinate centers of the black holes were located on the z axis: specifically, for the A1B8 computations, $\mathbf{C}_1/a_1 = (0, 0, 4)$ and $\mathbf{C}_2/a_1 = (0, 0, -4)$, while for the A2B8 series, $\mathbf{C}_1/a_1 = (0, 0, 4.046875)$ and $\mathbf{C}_2/a_1 = (0, 0, -3.953125)$.

C. Resolution parameters

For each method, and for each relevant model listed in Table I, we performed computations at three distinct resolutions—we generically refer to these computations as low, medium, and high resolution runs. Table II summarizes the values we used for the various numerical parameters which fix the resolution of each method. Recall from Sec. III A that the mesh structure for the Čadež algorithm is described by six parameters—$\mathcal{I}^+, \mathcal{I}^-, \mathcal{I}, \mathcal{S}^+, \mathcal{S}^-$, and $\mathcal{P}$. For this scheme, the design of the computational domain, coupled with the fact that meaningful results are attainable on relatively coarse meshes, makes a convergence test using a 4 : 2 : 1 ratio of the low : medium : high resolution scales natural and computationally tractable—thus, in going from a low-to-medium or medium-to-high calculation, all six of the Čadež mesh parameters are simply doubled.

As discussed in Sec. III B, a Cartesian computation is characterized by a single discretization scale, h, or equivalently, by the number of mesh points, n, on an edge of the computational cube, which, as the resolution is varied, has a fixed physical length. Here, computer resources limit our computations to a maximum $n \approx 128$ (we prefer $n = 16k$, for some integer k from hardware considerations), but solutions generated with $n \approx 32$ are *not* meaningful, so we have produced convergence series using a 2 : 3/2 : 1 relation of the low : medium : high resolution scales.

There is no single basic scale of discretization associated with the MQ method since the "grid" may have an arbitrary structure. For a fixed computational domain it is expected that by increasing the number of data points, N, the function to be evaluated will be sampled more densely and thus approximated more accurately (although there is no rigorous proof of this for general "grid" structures in multiple dimensions; see the discussion in Sec. IV E 1 below). Our choice of N in the MQ computations has been governed by constraints similar to those of the Cartesian approach. Below about $N = 800$ we find that the solution is poor due to insufficient sampling of the solution domain. Above $N = 2000$ the computation becomes very expensive because of the $O(N^3)$ operation count of the SVD algorithm. The low and high resolution values of N shown in Table III are representative of these two extremes. For comparison purposes the low : med : high resolution scale ratio can be written (for this 3D problem) in terms of $N^{-1/3}$, and is then given by 1.333 : 1.125 : 1.

D. Details of the comparison

Our comparison is itself comprised of two parts which are summarized in subsections IV E 1 and IV E 2 below. In both parts, errors (deviations) are computed at some set of $N_{\rm ref}$ *reference points*, labeled, for example, by their Cartesian coordinates, (x_i, y_i, z_i), $i = 1, \ldots, N_{\rm ref}$.

TABLE II. Parameters defining the various low-, medium- and high-resolution computations performed in the comparison.

Model	Res.	Čadež						Cartesian		MQ	
		$\mathcal{I}^+$	$\mathcal{I}^-$	$\mathcal{I}$ [a]	$\mathcal{S}^+$	$\mathcal{S}^-$	$\mathcal{P}$	n	h	N	$r_{\rm outer}/a_1$
A2B8TS	low	2	2	20(6)	8	8	16	64	0.450	842	730
A2B8	med.	4	4	40(12)	16	16	32	96	0.300	1402	730
A2B8NR	high	8	8	80(24)	32	32	64	128	0.225	1994	730
A1B8	low	2	2	24(8)	8	8	16	64	0.450	842	350
A1B8NR	med.	4	4	48(16)	16	16	32	96	0.300	1402	350
	high	8	8	96(32)	32	32	64	128	0.225	1994	350

[a] Values in parentheses are for the NR cases.

TABLE III. Norms of pointwise relative deviations in ψ using extrapolated Čadež values as reference except for A2B8TS where the reference solution is analytic.

		Čadež		Cartesian		Multiquadrics	
Model	Res.	$\|e\|_1$ (conv. rate)	$\|e\|_\infty$	$\|e\|_1$ (conv. rate)	$\|e\|_\infty$	$\|e\|_1$	$\|e\|_\infty$
A2B8TS	low	2.41×10^{-3}	1.06×10^{-2}	3.9×10^{-2}	1.9×10^{-1}	4.3×10^{-3}	4.0×10^{-2}
	med.	5.84×10^{-4} (2.04)	2.67×10^{-3}	1.5×10^{-2} (2.4)	1.0×10^{-1}	6.3×10^{-3}	2.7×10^{-2}
	high	1.45×10^{-4} (2.01)	6.29×10^{-4}	5.1×10^{-3} (3.7)	2.5×10^{-2}	3.1×10^{-3}	9.1×10^{-3}
	extrap.	3.12×10^{-6}	1.33×10^{-4}	—	—	—	—
A1B8	low	6.80×10^{-4}	5.19×10^{-3}	1.3×10^{-2}	4.5×10^{-2}	3.9×10^{-3}	6.9×10^{-2}
	med.	1.65×10^{-4} (2.04)	1.42×10^{-3}	1.3×10^{-2} (0.0)	4.4×10^{-2}	1.9×10^{-3}	3.6×10^{-2}
	high	4.13×10^{-5} (2.00)	3.54×10^{-4}	1.3×10^{-2} (−0.2)	4.4×10^{-2}	1.6×10^{-3}	2.6×10^{-2}
A1B8NR	low	1.43×10^{-3}	5.17×10^{-3}	2.3×10^{-3}	1.2×10^{-2}	—	—
	med.	3.48×10^{-4} (2.04)	1.42×10^{-3}	2.1×10^{-3} (0.3)	1.1×10^{-2}	—	—
	high	8.71×10^{-5} (2.00)	3.54×10^{-4}	2.0×10^{-3} (0.1)	1.1×10^{-2}	—	—
A2B8	low	7.13×10^{-4}	4.88×10^{-3}	1.2×10^{-2}	7.5×10^{-2}	7.7×10^{-3}	6.9×10^{-2}
	med.	1.69×10^{-4} (2.08)	1.57×10^{-3}	9.8×10^{-3} (0.5)	9.0×10^{-2}	4.6×10^{-3}	7.5×10^{-2}
	high	4.23×10^{-5} (2.00)	3.92×10^{-4}	6.3×10^{-3} (1.5)	2.0×10^{-2}	2.1×10^{-3}	2.7×10^{-2}
A2B8NR	low	1.74×10^{-3}	4.93×10^{-3}	8.9×10^{-3}	7.4×10^{-2}	—	—
	med.	4.12×10^{-4} (2.07)	1.58×10^{-3}	6.1×10^{-3} (0.9)	8.8×10^{-2}	—	—
	high	1.03×10^{-4} (2.00)	3.96×10^{-4}	2.7×10^{-3} (2.8)	1.4×10^{-2}	—	—

In both subsections, for those models where an analytic solution is not known (that is, for all models except A2B8TS), we define "error" as deviation from a reference solution generated from Richardson extrapolation of medium- and high-resolution Čadež results to the appropriate set of reference points. We remark that, in general, these points did not coincide with points actually used in the various "bare" Čadež, Cartesian, and MQ computations. Thus, some post-processing of *all* the basic results was generally necessary before the pointwise subtractions required to produce error estimates could be performed. We are confident, however, that we have, for the most part, succeeded in keeping the error due to post-processing small in comparison to the fundamental truncation errors of the various schemes, so that the reported levels of error are genuinely indicative of the level of error in the basic solutions.

In the first part of the comparison (Sec. IV E 1), the reference points were simply the points used in the various low-resolution Čadež computations. In this case, extrapolated values were generated using a two-step procedure: (1) the medium- and high-resolution values were interpolated to the reference points (interpolation was necessary due to the "zone-centered" nature of the Čadež differencing scheme), then (2) an appropriate linear combination of these interpolated values was formed to yield Richardson-extrapolated values at the reference points. In the second part of the comparison (Sec. IV E 2), the reference points were chosen to lie along that part of the z axis contained within the computational domain used in the Cartesian calculations. This is a region which is, in some sense, excluded from the Čadež computations (but has no particular significance for the other two methods) and, not surprisingly, this made the generation of extrapolated values somewhat more involved: (1) The high- and medium-resolution results were separately extrapolated (on the basis of Taylor, not Richardson, expansion) to the "natural" z-axis locations associated with their respective (η, ξ, ϕ) values; (2) the z-axis medium-resolution values were interpolated to the z-axis high-resolution points; (3) a linear combination of the z-axis medium- and the z-axis high-resolution values gave z-axis (Richardson) extrapolated values at "natural" z-axis high-resolution points; (4) a final interpolation along the z-direction produced values at the desired reference points.

Some care is required in producing such extrapolated results. All of the extrapolations are based on the premise that the solution $\psi^{\text{Čadež}}$, produced by the Čadež scheme, has the asymptotic ($h \to 0$) expansion

$$\psi^{\text{Čadež}} = \psi + h^2 e_2^{\text{Čadež}} + h^4 e_4^{\text{Čadež}} + \cdots , \qquad (61)$$

where h is the basic scale of discretization and $e_2^{\text{Čadež}}$, $e_4^{\text{Čadež}}$, ... are h-independent functions. In the limit $h \to 0$, we expect output from the Čadež algorithm to adhere more and more accurately to (61) *on the Čadež grid points*. In order to produce two-level extrapolated results at a *different* set of points, we must ensure that we interpolate the "bare" results to sufficiently high order that we preserve the first two terms of (61). For example, in the two-step procedure described above, *linear* ($O(h^2)$) interpolation of the medium- and high-resolution results to the low-resolution grid points would be insufficient since that procedure would introduce new $O(h^2)$ terms which, except for special mesh geometries, would not be (significantly) "cancelled" by Richardson extrapolation. In order to interpolate both ψ and $h^2 e_2^{\text{Čadež}}$ correctly, we

need to use at least *quadratic* ($O(h^3)$) interpolation. In the generation of *all* of our Richardson-extrapolated reference results we have been conservative in our interpolation and (polynomial-)extrapolation operations, invariably using a higher order of interpolation than is strictly necessary.

As mentioned above, the various "bare" results which were produced by running each code-model pair at three different resolutions also had to be post-processed in order to produce values at the specific sets of reference points just described. The Čadež values were (again conservatively) cubically ($O(h^4)$) interpolated to the reference locations, while linear interpolation was employed for the Cartesian quantities (fundamental considerations and direct numerical experiments indicate that the $O(h^2)$ errors incurred by the linear interpolation are negligible in comparison to the truncation error of the scheme). We also note that we made no attempt to compute errors in the Cartesian results at points which lie outside the (rather small) Cartesian computational domain. Finally, the functional-approximation nature of the MQ provides a natural mechanism for producing a numerical solution value at any point within the MQ computational domain—Eq. (55) was simply evaluated at arbitrary (x, y, z) using the appropriate set of numerically computed basis coefficients.

In Sec. IV E 1, we quantify the basic level of error in any of the numerical computations ψ^{model} in terms of the following discrete ℓ_1 and ℓ_∞ norms of the relative deviation from the reference solution ψ^{ref}:

$$\|e\|_1 \equiv \frac{1}{N'_{\text{ref}}} \sum_{i=1}^{N'_{\text{ref}}} \frac{|\psi_i^{\text{model}} - \psi_i^{\text{ref}}|}{\psi_i^{\text{ref}}}, \tag{62}$$

$$\|e\|_\infty \equiv \max_{i=1}^{N'_{\text{ref}}} \frac{|\psi_i^{\text{model}} - \psi_i^{\text{ref}}|}{\psi_i^{\text{ref}}}, \tag{63}$$

where the index i in these expressions ranges over the N'_{ref} of the N_{ref} values which lie within the computational domain of the particular calculation under consideration. For the finite difference solutions, we also estimate a convergence rate by computing the ratio

$$\frac{\ln\left(\|e^{h_1}\|_1 / \|e^{h_2}\|_1\right)}{\ln(h_1/h_2)} \tag{64}$$

where h_1 and h_2 are the low and medium, or medium and high resolution discretization scales. Clearly, in the limit $h_1, h_2 \to 0$, this ratio should approach p for an $O(h^p)$ difference scheme.

E. Results of the comparison

1. *Global error analysis*

The results of the first part of our comparison are summarized in Table III; here we make a few additional comments about overall features of the comparison as well as the general performance of individual methods. In the first place, and perhaps most importantly, we observe that the tabulated results show a satisfying level of agreement among the output of the various numerical schemes. For all three methods, we generally have average agreement of the high resolution results to within 1% or so, and for most of the calculations, there is a general trend of decreasing deviation with increasing resolution.

In addition to this overall agreement, the superior accuracy of the Čadež results in comparison to the results from the other two methods is also striking. Particularly noteworthy is the clear $O(h^2)$ convergence manifested by all of the Čadež computations; this convergence behavior is significantly better than that of either of the other two algorithms and, as a result, the high-resolution Čadež results are generally well over an order of magnitude (and in some instances nearly two orders) more accurate than the best Cartesian or MQ results. Furthermore, as previously discussed, because of this rather precise $O(h^2)$ convergence, the Čadež results can be substantially improved using Richardson extrapolation. For example, Table III shows that for the time-symmetric computation (A2B8TS), two-level extrapolation provides nearly a 500-fold improvement on the accuracy of the high-resolution results (the improvement in the ℓ_∞ norm is not so dramatic, but we have not studied this issue in any detail). Based on the similarity of the observed levels of deviation in the Čadež results from model to model, we conclude (self-consistently) that the other extrapolated solutions (reference solutions) have similar accuracy.

In contrast to the Čadež results, the general convergence properties of the Cartesian data sets are more difficult to assess and quantify. As anticipated in Sec. III B, we believe that the somewhat erratic convergence behavior of the method seen in Table III is largely attributable to (1) The nature of our approximation of the inner boundary conditions [which are generally $O(h)$ accurate while the discretization of the interior equations is $O(h^2)$], and (2) the small diameter of the Cartesian computational domain. The A1B8NR and A2B8NR models were introduced specifically to estimate the relative effect of this second aspect of the Cartesian computations on the overall level of error. As can be seen from Table III, errors in the Cartesian results in comparison to the NR reference solutions *are* significantly less than the deviations from the solution of the corresponding base model. In addition, the Cartesian convergence rates of the NR data sets are clearly superior for both the A1B8 and A2B8 models. For a model like A1B8 the error induced by imposing the outer boundary condition at such a small radius is a significant (if not dominant) fraction of the total error, even for the low-resolution computation.

A rigorous analysis of the convergence behavior of the MQ results is difficult. In the case of a 1D, uniform, infinite grid some quantitative results have been found [23]. The convergence rate under such idealized conditions is exponential (as in pseudospectral methods). In the general case, however, the convergence behavior appears to be a function, not only of N, but also of the arbitrary parameters $s_{\min/\max}$ and the form of the functions to be solved for. An experiment on the convergence behavior of the scheme when applied to the single-black-hole initial-data problem was presented in Ref. [20]. There,

a general trend of increasing accuracy with increasing N and ratio $s_{\max}/s_{\min}$ was found. Unfortunately, as both of these parameters increase so does the condition number of the matrix. For any given precision of floating-point arithmetic, there comes a point when the matrix condition number is so high as to render its solution meaningless. Even before this extreme situation is reached the solution deteriorates due to loss of significant figures. Therefore, increasing N and $s_{\max}/s_{\min}$ does not produce a monotonic increase in accuracy (at least for the solution method described here).

2. *z-axis error analysis*

The second part of our comparison focused on one particular model (A1B8), and a set of about 130 reference points lying along the z axis ($x = y = 0$) within the domain of the Cartesian computations. The results of this comparison are summarized in Figs. 4–8. Figure 4 shows a superposition of the data from all three high-resolution runs of the A1B8 model (symbols are plotted at every third reference point). Apart from the slight deviation of the Cartesian results for larger values of $|z|$, differences among the solutions are not discernible on the scale of the graph. Figures 5–8 show detailed views of the convergence behavior of the various methods along the z axis. Note that the vertical scales of Figs. 5–6 and 8 are identical, while that of Fig. 7 is about half that of the others.

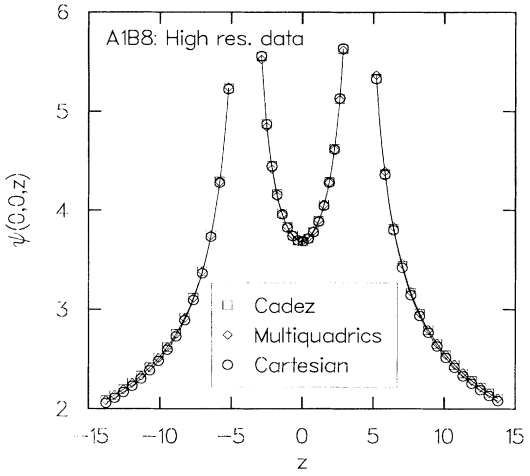

FIG. 4. Superposition of high-resolution Čadež, multiquadrics and Cartesian results along the z axis for model A1B8. See Tables I and II for model and resolution parameters respectively, and refer to the text for discussion of the post-processing that was applied to each "raw" high-resolution data set in order to produce a cut along the z axis. Observe that differences among the various solutions are not visible on the scale of this graph, except at larger values of $|z|$—near the edges the Cartesian computational domain—where the Cartesian results show a slight deviation. In this and subsequent figures, symbols are plotted every third data point.

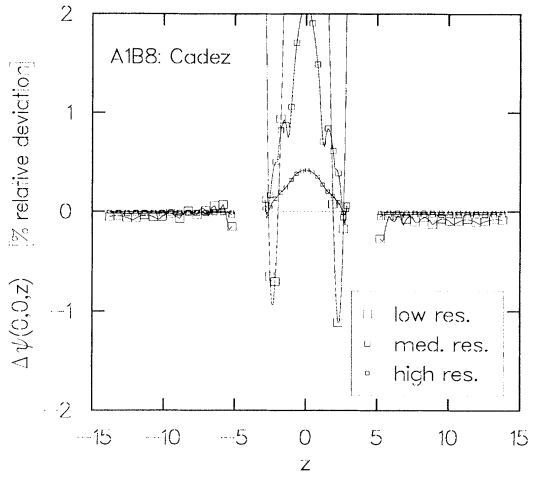

FIG. 5. z-axis convergence series of the Čadež computations for model A1B8. In this and subsequent figures, deviations are computed with respect to reference results generated using the four-step Richardson-extrapolative procedure described in the text. Here the rapid [quantitatively $O(h^2)$] and regular convergence characteristic of *all* of the Čadež calculations performed in our comparison is evident. Note that the relative deviations are largest in the vicinity of the Čadež singularity, which for model A1B8 is located at $(0,0,0)$.

In Fig. 5 the rapid [quantitatively $O(h^2)$] convergence of the Čadež data is again apparent. (Some of the low-resolution deviations have been clipped, but without any significant loss of information since the convergence is so good.) We remark that the figure presents a somewhat less glowing assessment of the accuracy of the Čadež re-

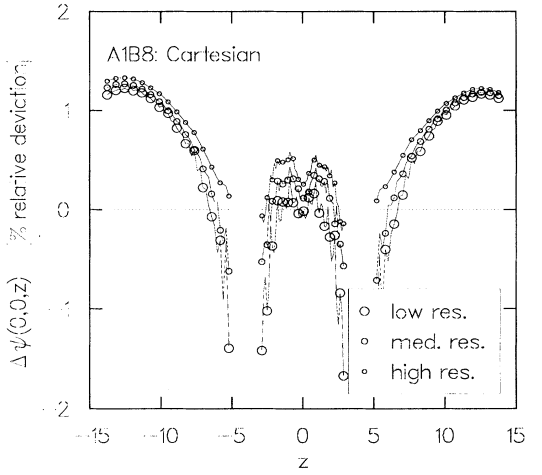

FIG. 6. z-axis convergence series of the Cartesian computations for model A1B8. Although a general trend of decreasing error with increasing resolution can be seen in this plot, the effect of the small computational domain used in this and the A2B8 and A2B8TS Cartesian calculations is clear—the accuracy is limited not by poor resolution, but by the approximate nature of the outer boundary condition (7), imposed here at $r \approx 15$.

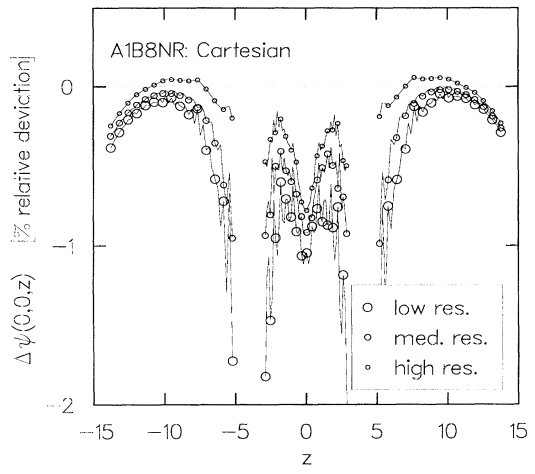

FIG. 7. z-axis convergence series of the Cartesian computations for model A1B8NR. Here the reference solution was generated by Richardson-extrapolating Čadež results for model A1B8NR where the outer boundary condition (7) was applied at $r \approx 17$ to roughly coincide with the radius at which the condition was imposed in the Cartesian calculations. As expected, in comparison to the previous figure, the convergence of the Cartesian results is substantially improved (note the reduced vertical scale of this plot).

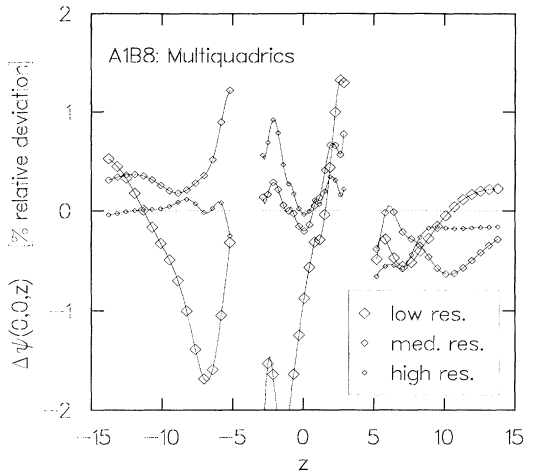

FIG. 8. z-axis convergence series of the multiquadrics computations for model A1B8. As with Fig. 6, there is an overall trend of decreasing error with increasing resolution. However, as discussed in the text, analysis of the convergence of the MQ scheme is complicated by the influence of adjustable parameters other than the number of data points, N.

sults than does Table III. (Recall that the error norms reported in Table III were computed using sets of reference points naturally associated with the low resolution Čadež calculations.) Indeed, we find that the basic level of relative error observed along the z axis in Fig. 5—in the vicinity of the holes, and particularly near the Čadež singularity—is at least an order of magnitude worse than the tabulated errors. Although we have not studied the issue in detail, this "amplification" of the level of error seems quite plausible given the nature of the Čadež coordinates and the fact that the z axis is not naturally well represented in this system. However, the "continuation" of any basic numerical solution to an arbitrary point within the bounds of a computational domain can be of considerable interest in general, and, in this regard, we feel that the deviations seen in Fig. 5 represent characteristic levels of "worst-case" error for the Čadež calculations.

Figures 6 and 7 show errors along the z axis in the various Cartesian solutions of the A1B8 and A1B8NR models, respectively. It is clear from Fig. 6 (as well as Fig. 4) that the errors in the A1B8 calculation are proportionately largest near the outer boundary of the computational domain, particularly for the highest resolution calculation. When errors are computed using the A1B8NR reference solution (Fig. 7), there is a significant reduction in the overall level of error at all resolutions (which is also apparent from the results listed in Table III) and visibly better convergence behavior.

Finally, Fig. 8 displays the pointwise errors of the various multiquadrics results along the z axis. Again, it is currently difficult for us to make any quantitative statements concerning the convergence of the MQ method. We generally observe smaller relative errors at higher resolutions (in accord with the results in Table III), but, for example, the errors between the holes in the medium-resolution calculation are significantly less than the corresponding errors in the high-resolution data. We also note that the forms of the error functions show little correlation with the solution ψ (or derivatives of ψ); this is perhaps to be expected given the global nature of the MQ method.

V. CONCLUSIONS

It is clear that all three of the methods described in this paper can construct useful initial-data sets to be used in the simulation of black-hole collisions. Each method, however, has its strengths and weaknesses both from the point of view of simply constructing initial-data sets and for the eventual evolution of a prescribed system.

For the task of constructing an initial-data set as accurately as possible for a given amount of computational effort, the Čadež approach is undoubtedly the best choice. Its one shortcoming is the lower resolution and accuracy of the region between the two holes, near the Čadež singularity. This shortcoming can, however, be alleviated with the use of an adaptive-gridding algorithm to increase the grid resolution in this area. With the eventual move to time evolutions of these initial-data sets in mind, the need to consider alternatives to the Čadež approach is apparent. The numerical instabilities which are often associated with evolution schemes built upon curvilinear coordinates like those of Čadež must be considered as a significant threat to the eventual success of any "Čadež" evolution scheme. While the Čadež approach should not be abandoned, alternative approaches which can avoid numerical instabilitites associated with coordinate sin-

gularities *should* be investigated.

Both the Cartesian and the MQ approaches described in this paper are free of coordinate singularities and may provide effective alternatives to the Čadež approach. For the first time in the field of numerical relativity, a Cartesian coordinate system has been successfully used in a problem with "nontrivial" boundary topologies. The uniform gridding used at present, however, produces a distribution of grid points which is far from ideal. This is the cause of the two major shortcomings of the Cartesian approach described here: the relatively low resolution near the inner boundaries which hinders the accuracy of imposing the inner boundary condition and the necessity of positioning the outer boundary at too close a "radius." As with the Čadež approach, the use of adaptive gridding should provide an effective means of addressing both of these problems.

Finally, the MQ method remains as an intriguing alternative approach. This global, spectral-like scheme may provide a uniquely different approach to the problem of evolving the collision of two black holes. As described here, the major drawback is the ill conditioning of the matrix system to be solved. Recent work, however, indicates that by using a more sophisticated implementation of the MQ method, incorporating domain decomposition and blending techniques [27], the ill-conditioning problem can be eliminated. Moreover, the number of operations required to solve the system is then substantially reduced and larger numbers of data points may be used to give higher accuracy.

ACKNOWLEDGMENTS

M.R.D. acknowledges financial support from NATO/SERC. S.R.O. was supported in part by CAPES-Brazilian Education Council and Universidade de Brasilia, Brazil. This work was supported in part by the National Science Foundation under Grant Nos. PHY-9007834 at Cornell and PHY-8806567 at Texas. Computations in support of this research were performed at the Cornell National Supercomputing Facility, which was supported in part by the National Science Foundation, IBM Corporation, New York State, and the Cornell Research Institute, and at the Center for High Performance Computing, University of Texas System. Richard Matzner acknowledges a Cray University Research grant and support under Texas Advanced Research Program grant TARP-085.

[1] A. Čadež, Ph.D. dissertation, University of North Carolina, 1971; L. L. Smarr, Ph.D. thesis, University of Texas at Austin, 1975; K. R. Eppley, Ph.D. thesis, Princeton University, 1975; L. L. Smarr, A. Čadež, B. DeWitt, and K. Eppley, Phys. Rev. D **14**, 2443 (1976); L. L. Smarr, in *Eighth Texas Symposium on Relativistic Astrophysics*, edited by M. D. Papagiannis (The New York Academy of Sciences, New York, 1977); P. Anninos, D. Bernstein, E. Seidel, L. Smarr, and D. Hobill, in *Abstracts of Contributed Papers: 13th International Conference on General Relativity and Gravitation*, edited by P. W. Lamberti and O. E. Ortiz (FAMAF, Cordoba, Argentina, 1992).

[2] J. Thornburg, Class. Quantum Grav. **4**, 1119 (1987).

[3] G. B. Cook, Phys. Rev. D **44**, 2983 (1991)

[4] J. W. York, Jr., in *Sources of Gravitational Radiation*, edited by L. L. Smarr (Cambridge University Press, Cambridge, England, 1979).

[5] J. Bowen, Gen. Relativ. Gravit. **11**, 227 (1979); J. Bowen and J. W. York, Jr., Phys. Rev. D **21**, 2047 (1980); J. Bowen, Gen. Relativ. Gravit. **14**, 1183 (1982).

[6] A. D. Kulkarni, L. C. Shepley, and J. W. York, Jr., Phys. Lett. **96A**, 228 (1983).

[7] R. Arnowitt, S. Deser, and C. W. Misner, in *Gravitation: An Introduction to Current Research*, edited by L. Witten (Wiley, New York, 1962).

[8] J. Bowen, J. D. Rauber, and J. W. York, Jr., Class. Quantum Grav. **1**, 591 (1984).

[9] R. L. Hardy, J. Geophys. Res. **76**, 1905 (1971); R. L. Hardy, Comput. Math. Applic. **19**, 163 (1990)

[10] M. W. Choptuik, D. S. Goldwirth, and T. Piran, Class. Quantum Grav. **9**, 721 (1992).

[11] J. M. Centrella, S. L. Shapiro, C. R. Evans, J. F. Hawley, and S. A. Teukolsky, in *Dynamical Spacetimes and Numerical Relativity*, edited by J. M. Centrella (Cambridge University Press, Cambridge, England, 1986).

[12] A. Einstein and N. Rosen, Phys. Rev. **48**, 73 (1935).

[13] J. W. York, Jr. and T. Piran, in *Spacetime and Geometry: The Alfred Schild Lectures*, edited by R. Matzner and L. Shepley (University of Texas Press, Austin, 1982).

[14] Note that Eq. (B7) in [3] is in error. The case "1 for $n = 1$" should read "α^{-1} for $n = 1$."

[15] A. Brandt, Math. Comput. **31**, 333 (1977); M. W. Choptuik and W. G. Unruh, Gen. Relativ. Gravit. **18**, 813 (1986); G. B. Cook, in *Frontiers in Numerical Relativity*, edited by C. R. Evans, L. S. Finn, and D. W. Hobill (Cambridge University Press, London, 1989).

[16] R. S. Varga, *Matrix Iterative Analysis* (Prentice-Hall, Englewood Cliffs, NJ, 1962).

[17] R. Franke, Math. Comput. **38**, 181 (1982); N. Dyn, D. Levin, and S. Rippa, SIAM J. Sci. Stat. Comput. **7**, 639 (1986); C. A. Micchelli, Constr. Approx. **2**, 11 (1986).

[18] A. E. Tarwater, "A Parameter Study of Hardy's Multiquadric Method for Scattered Data Interpolation," Report UCRL-54670 (1985); R. E. Carlson and T. A. Foley, Comput. Math. Applic. **21**, 29 (1991).

[19] E. J. Kansa, Comput. Math. Applic. **19**, 127 (1990); **19**, 147 (1990).

[20] M. R. Dubal, Phys. Rev. D **45**, 1178 (1992).

[21] M. R. Dubal, S. R. Oliveira, and R. A. Matzner, in *Approaches to Numerical Relativity*, edited by R. d'Inverno (Cambridge University Press, Cambridge, England, 1992).

[22] C. W. Misner, Ann. Phys. (N.Y.) **24**, 102 (1963).

[23] M. J. D. Powell, in *Advances in Numerical Analysis II: Wavelets, Subdivision Algorithms and Radial Functions*, edited by W. Light (Oxford University Press, Oxford, England, 1991).

[24] W. H. Press, B. P. Flannery, S. A. Teukolsky, and

W. T. Vetterling, *Numerical Recipes: The Art of Scientific Computing* (Cambridge University Press, Cambridge, England, 1986).
[25] J. Stoer and R. Bulirsch, *Introduction to Numerical Analysis* (Springer-Verlag, Berlin, 1980).
[26] G. B. Cook and A. M. Abrahams, Phys. Rev. D **46**, 702 (1992).
[27] E. J. Kansa, Comput. Math. Applic. **24**, 169 (1992).